

# Large Eddy Simulation of the Flow Around an Airfoil

Simon Dahlström and Lars Davidson

Department of Thermo and Fluid Dynamics, Chalmers University of Technology, Gothenburg

This report deals with the use of Large Eddy Simulation (LES) applied on a high-Reynolds flow around a profile close to stall. These simulations have been conducted on the IBM SP computer at PDC. The work has been a part of the LESFOIL project and is presently a part of the FLOMANIA project.

## Airfoil Condition

Figure 1 shows the airfoil (the Aerospatiale A-profile) that has been studied. The front part of the airfoil is called the leading edge and the rear part is the trailing edge. The chord of the airfoil,  $c$ , is the distance from the leading to the trailing edge. The upper side of an airfoil is called the suction side and the lower the pressure side. The angle of attack,  $\alpha$ , is the angle between the chord line and the freestream velocity,  $U_\infty$ .

Measurements of this flow have been carried out in two wind tunnels, the F1 and F2 wind tunnels at Onera [1]. A range of flow data was collected in these experiments, at different Reynolds numbers and at different angles of attacks. However, the case studied in the LESFOIL project, was the  $13.3^\circ$ -case and based on the freestream velocity and the chord of the airfoil the Reynolds number,  $Re_c = U_\infty c / \nu$ , is equal to 2 million. The flow is subsonic with a freestream Mach number of 0.15. In both experiments the boundary layer was tripped at 30% of the chord on the pressure side. In Figure 2 experimental results of the lift and drag versus the angle of attack are shown. The dashed line marks the  $13.3^\circ$ -case and we see that the flow is near maximum lift and the airfoil is close to stall.

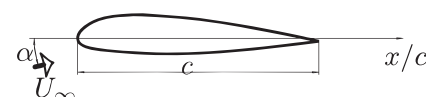


Figure 1  
Aerospatiale A-profile.

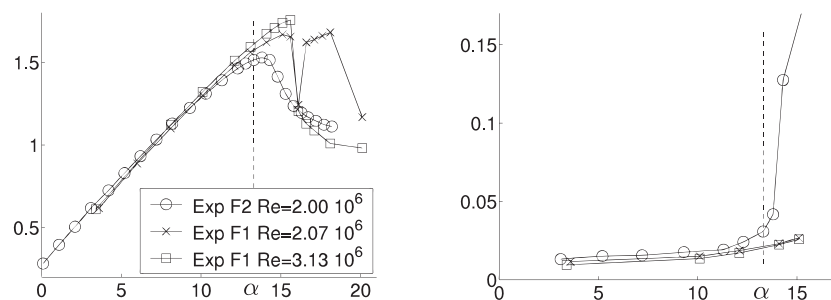
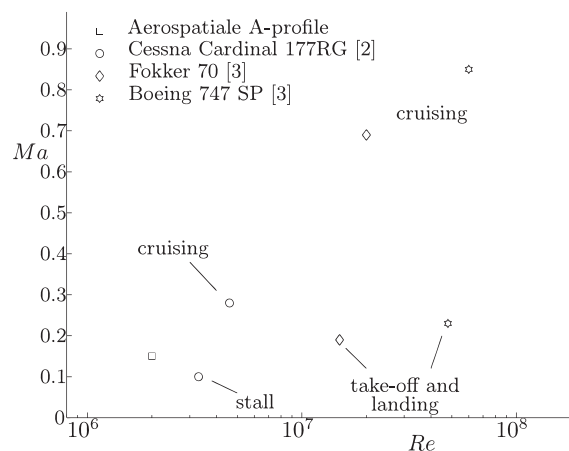


Figure 2  
Lift and drag coefficients versus the angle of attack.

In Figure 3 the set-up condition for the Aerospatiale A-profile at  $Ma = 0.15$  and  $Re = 2 \cdot 10^6$  is compared to different conditions for some airplanes. The set-up condition is in the region where stall, take-off and landing occur for a small airplane, such as the Cessna (it differs a factor of approximately 2). Comparing with a large aircraft, such as Boeing 747, the Reynolds number is almost 25 times higher than in the Aerospatiale case, although still in the region where incompressible methods (such as those used in the present report) apply. The required resolution and the computer resources needed at this much higher Reynolds number are estimated later in this report for smooth 2D and 3D wings.

Figure 3  
Take-off, landing, stall and cruising conditions for some aeroplanes and the set-up condition for the Aerospatiale A-profile.



### Large eddy simulation of the airfoil flow

In LES the large-scale eddies are resolved and the small scales are modeled. The uncertainty of the modelling is reduced when the important large scales are resolved. This is the case with wall-resolved large-eddy simulations, where the important near-wall structures are partly resolved. These structures are large compared to the small-scale turbulence in this region, however, they are not large, compared to other length scales in the outer part of a boundary layer and wall-resolved simulations are often not a feasible alternative because they are far too expensive to perform.

Instead, in the high-Reynolds flow around the airfoil, the minimum requirements in order to conduct an LES are investigated. In this approach the near-wall region is to be modeled and the question is: what resolution is required in the region outside the near-wall region? The minimum requirement is to resolve large flow structures such as boundary layers, separation bubbles etc., with a sufficient amount of nodes. However, what needs to be stressed, is that the largest scale in a flow could be very small. Looking at the different types of flows around an airfoil,

both the laminar and the turbulent boundary layers could be very thin and so could the separation bubbles.

In LES the filtered (time-dependent) Navier-Stokes equations are solved. LES thus gives information about the transients of the flow and the simulations give a physical representation of the flow as the time progresses. This feature of LES can be used to visualize the different flow regions around the Aerospatiale A-profile. Because of the shape of the airfoil and the angle of attack the flow streams faster on the suction side of the profile. Bernoulli's equation states that this means low pressure and the opposite on the pressure side: lower velocity and an increase in the pressure. This is the mechanism that makes the airfoil lift. In Figure 4 we see the pressure distribution around the A-profile. Dark color is low pressure and lighter is high. Almost all over the suction side the pressure is lower than the freestream pressure, especially in the region around the leading edge, where there is a pressure peak. At approximately 20 % of the chord and downstream the pressure fluctuates: the pressure decreases or increases locally resulting in eddies or swirls in the flow. Here in this region the flow is turbulent.

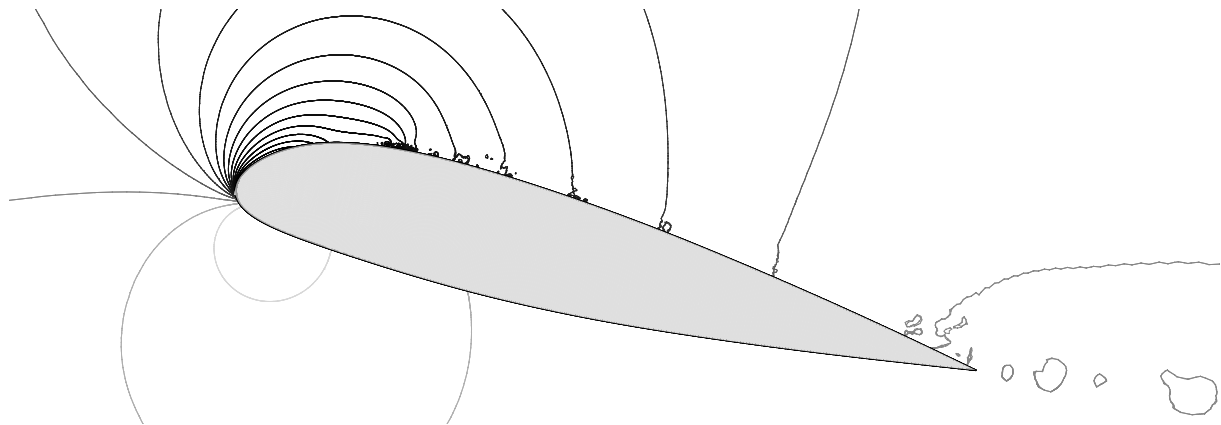


Figure 4  
Pressure contours.

In Figure 5 the different flow regions around the airfoil are illustrated. The stagnation point region and a part of the very thin laminar boundary layer are shown. The mesh used consists of  $1393 \times 127$  grid nodes in the streamwise and wall-normal direction respectively and in order to resolve the laminar boundary layer the height of the cell at the leading edge is as small as  $5 \cdot 10^{-6}c$ .

On the suction side, there is a peak in the pressure gradient near the leading edge. The favorable pressure gradient accelerates the flow around the leading edge. Figure 5 also shows streamlines in the transitional region. In the left part of this

sub figure the streamlines do not fluctuate, i.e. the boundary layer is laminar and then a separation bubble is formed. Inside of this bubble, the streamlines look more chaotic and a transition is taking place. When the flow reattaches the streamlines fluctuate and the boundary layer is turbulent. Here in the transitional region the resolution needs to be fine in the streamwise direction in order to capture the transition and the reattachment of the bubble.

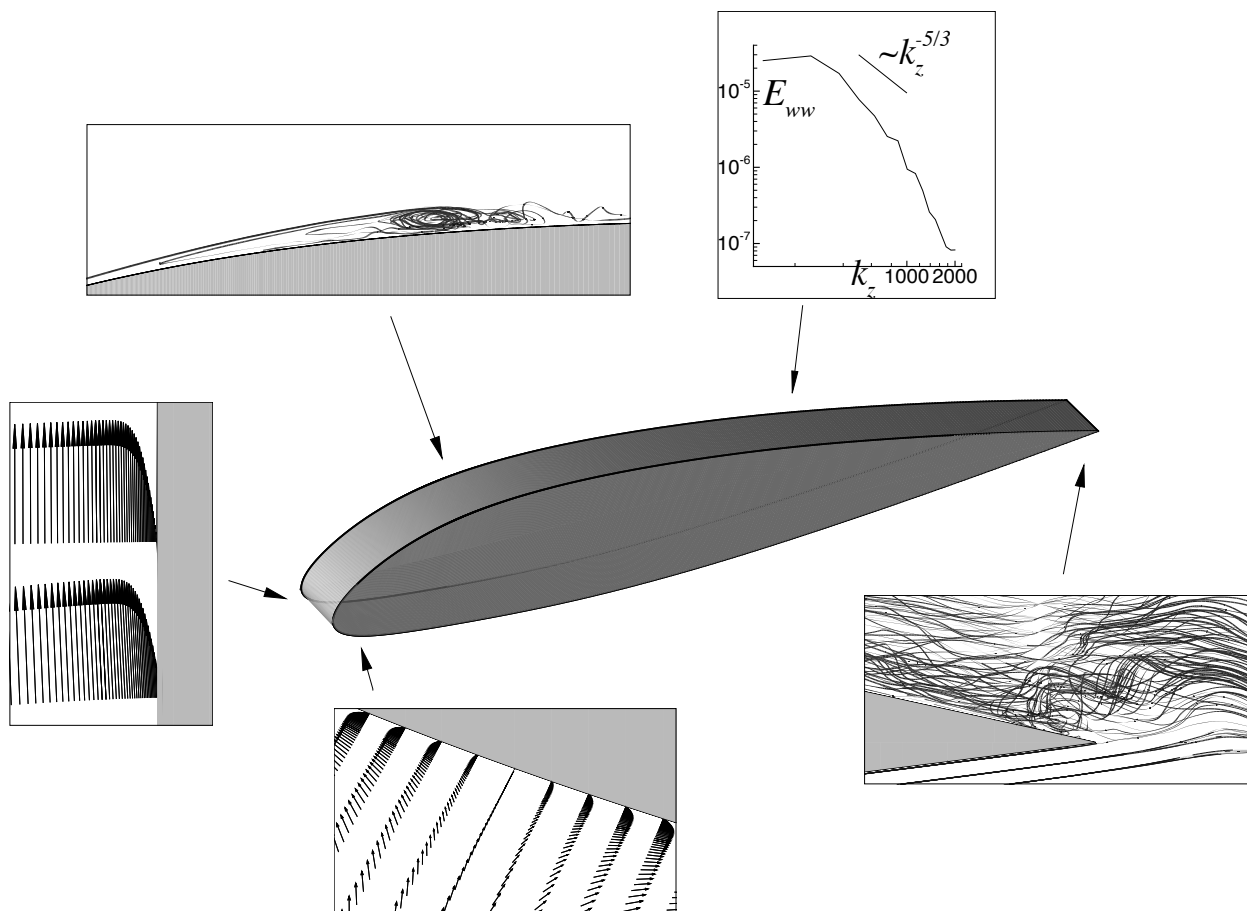


Figure 5  
Instantaneous contour plot of the spanwise velocity, streamlines, velocity vectors and energy spectra, illustrating the different flow regions around the Aerospatiale A-profile.

Also shown in Figure 5 is an energy spectra taken at a point in the turbulent boundary layer. The large eddies are resolved and the cut-off is in a  $-5/3$ -range region. The resolution on this mesh is less than approximately 200 wall units or

$N_x \approx N_z \approx 8$ . Here  $N_x$  and  $N_z$  are the number of nodes per boundary layer thickness,  $\delta$ , in the streamwise and spanwise direction, respectively. Since the boundary layer thickness is not expected to change much as the Reynolds number increases, this later estimation, is an estimation of the required resolution, which is fairly independent of the Reynolds number.

Figure 5 also shows a side view of streamlines in the trailing edge region and a small separation bubble is seen. When the angle of attack increases, this bubble gets larger and finally the airfoil stalls and loses its lift.

In Figure 6 a rear view of streamlines illustrates the turbulent boundary layer and the eddies (or swirls) that are present at an instant in this region. The fluctuations get more intense in the turbulent boundary layer in the region close to the airfoil.

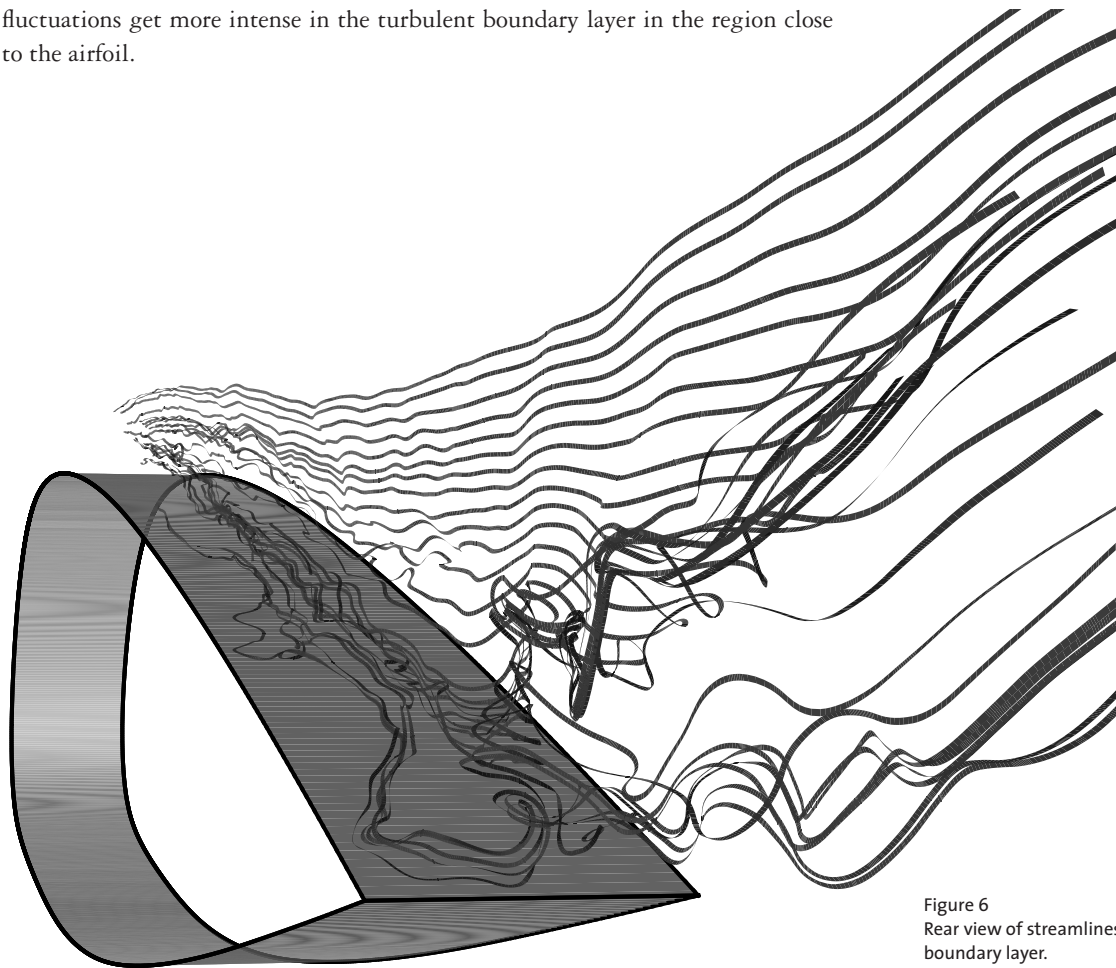


Figure 6  
Rear view of streamlines in the turbulent boundary layer.

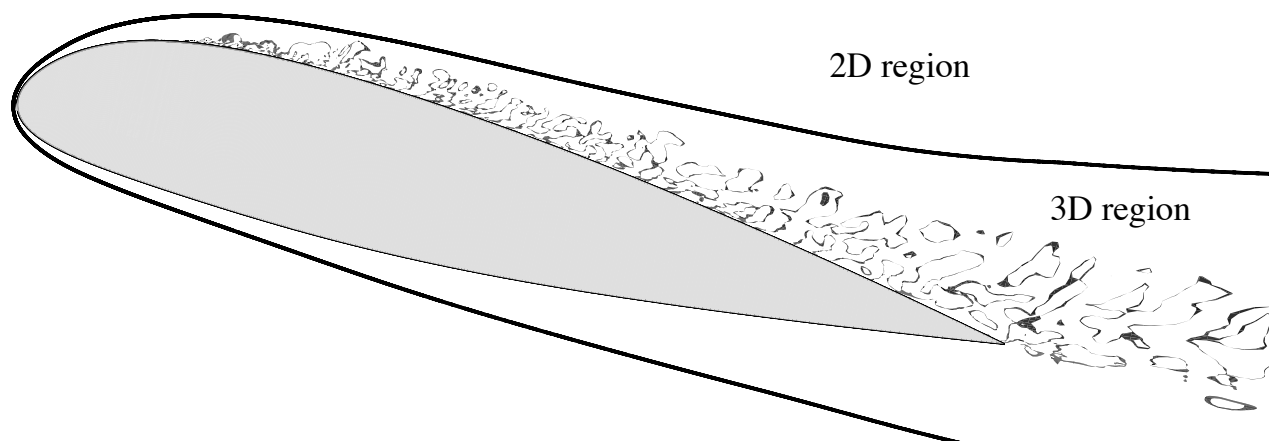
## Parallelisation

In the simulations an estimate of the boundary layer thickness has been used to decrease the number of nodes by using a 2D/3D approach. On a sufficient distance outside turbulent regions only 2D simulation is performed (the spanwise amount of nodes is 3). In the 3D region, 33 nodes are used. This 2D/3D approach, which was used by ONERA [4], saves 45% of the nodes. In Figure 7 the matching line between the 2D region and the 3D region is shown. The turbulent region seems to be dangerously close to the matching line, e.g. at 30% of the chord, however in this particular simulation the boundary layer thickness is overpredicted, much because of a too large transitional separation bubble in the simulations.

The computations have been performed on an IBM SP computer at PDC. MPI is used as the message passing system and the computational domain is decomposed into 36 subdomains:  $4 \times 2 \times 4$  in the 3D domain and  $4 \times 1 \times 1$  in the 2D domain. Dirichlet boundary conditions are used between the blocks.

The code used is an incompressible finite volume Navier-Stokes solver called CALC-BFC (Davidson and Farhanieh [5]). The solver is based on structured grids and the use of curvi-linear boundary fitted coordinates.

Figure 7  
The choice of the 2D/3D interface on the Chalmers II mesh and contour levels of the spanwise velocity (1% of the freestream velocity).



## Estimation of required computer power

Here the future of LES is discussed, especially the requirements on LES in order to compute flows around wings. Also the importance of near-wall modeling (such as hybrid RANS/LES) is stressed. In [6] Spalart estimates the feasibility of different methods and at what year the methods are ready. Here similar estimates are done, however with the coarse simulations presented in this report as a base.

### Resolution at $Re = 2 \cdot 10^6$

So, what are the characteristics of the present simulations? The mesh consists of 3.2 million nodes, the spanwise distance is 5% of the chord and an averaging time of  $10c/U_\infty$  is regarded as sufficient. With a time step of  $1 \cdot 10^{-4}c/U_\infty$ , the required nodes in space and time are  $3.2 \cdot 10^{11}$ . Now supposing the present coarse LES approach should be applied on a 3D wing with a span of 8 chords, the total amount of nodes would be 512 million (it is a factor of 160 larger, compared to the present 2D profile with a spanwise distance of  $0.05c$ ). As in [6], 6 spans of averaging is regarded as necessary for a wing, however the same time step can be used as for the 2D profile and the required nodes in space and time becomes  $2.5 \cdot 10^{14}$ .

### Resolution at higher Reynolds numbers

In order to estimate the required resolution when the Reynolds number increases the resolution has to be related to this number. For the amount of nodes in the streamwise and spanwise direction, the following is assumed for an airfoil (with at most incipient separation near the trailing edge and  $Re = U_\infty c/\nu$ ):  $N_x^{tot} \sim \frac{Re^{0.9305}}{\Delta x^+}$ ,  $N_z^{tot} \sim \frac{Re^{0.9305}}{\Delta z^+}$  and that  $N_y^{tot}$  is independent of the Reynolds number. The CFL number should be constant (and less than one) and the number of time steps,  $N_t$ , becomes:  $N_t \sim \frac{Re^{0.9305}}{\Delta x^+}$ . For more details see [7].

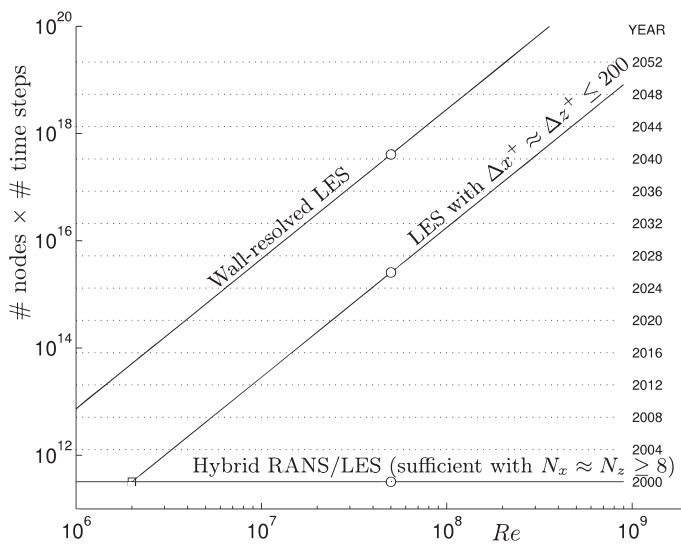


Figure 8  
Estimates for 2D wing-profile computations. Square: the present computation; circles: the “real-life” Reynolds number at take-off and landing.

## Discussion

The present parallel's simulations of the flow around the 2D airfoil are viewed as most feasible (regarding the computing time, not regarding the accuracy) in the year of 2000. This coarse approach is not ready, since it lacks accuracy in the modeling of the near-wall region and the treatment of the laminar region. Further, time will tell if it is sufficient with an amount of 8 nodes per boundary layer thickness just downstream of the transition ( $N_x \approx N_z \approx 8$ ), as is the case in the present computations.

Three different roads are marked in Figure 8:

- Wall-resolved LES with  $\Delta x^+ = 50$  and  $\Delta z^+ = 20$  just downstream of the transition.
- Wall-function resolution: a resolution of 200 wall units ( $\Delta x^+ \approx \Delta z^+ \approx 200$ ) and 8 nodes per boundary layer thickness downstream of the transition at  $Re = 2 \cdot 10^6$ .
- Hybrid RANS/LES resolution:  $y_1^+ < 1$  and  $N_x \approx N_z \approx 8$  downstream of the transition.

The year scale is based on that the computer power increases by a factor of two every second year. If there are requirements on the resolution in wall units, the total amount of nodes in space and time are strongly dependent on the Reynolds number, as seen in the figure. With the estimates above the resolution in space and time scales like  $Re^{2.79}$  for wall-resolved LES and the LES with wall-unit requirements on the wall-function resolution. These methods are referred to by Spalart et al. as Quasi-DNS (QDNS) methods [8]. If, the near-wall problem is solved, i.e. there are no requirements on the near-wall resolution in wall units, the amount of nodes becomes rather Reynolds independent (if the boundary layer thickness does not increase much). This case is marked with a horizontal line in Figure 8. As the Reynolds number increases, the crucial difference between this approach and QDNS approaches is illustrated in the figure. The possible road seems to be to use the hybrid RANS/LES approach in order to conduct simulations at the "real-life" Reynolds numbers. Here the resolution only needs to be refined in the wall-normal direction and the number of nodes scales like  $\ln(Re)$ .

Figure 9 shows the estimations for a 3D wing together with an estimate from [8], where  $N_0 = N_x = N_y = N_z = 20$ , an unstructured grid is used and the boundary layer is turbulent from the attachment line. This high estimate demonstrates how very thin the boundary layer around the leading edge is. Further, it is assumed that the near-wall problem is solved.

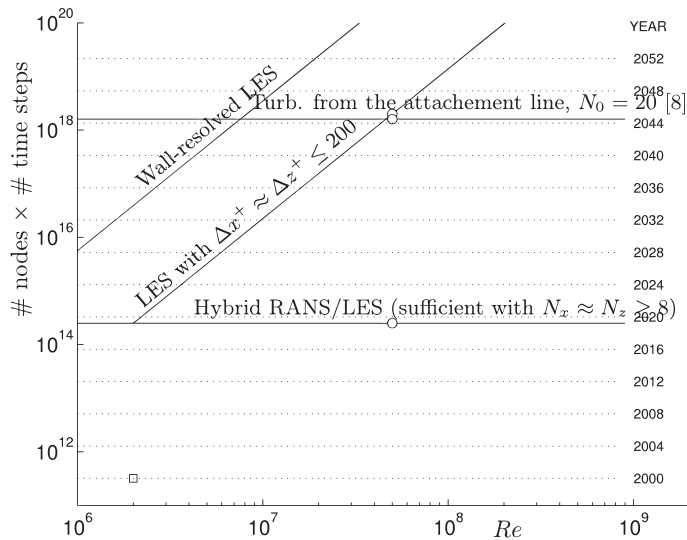


Figure 9  
Estimates for 3D wing computations.  
Square: the present computation; circles: the  
"real-life" Reynolds number at take-off and  
landing.

## References

1. E. Chaput. Aerospatiale-A Airfoil. Contribution in ECARP- European Computational Aerodynamics Research Project: Validation of CFD Codes and Assessment of Turbulence Models. In W. Haase *et al.*, editor, *Notes on Numerical Fluid Mechanics*, volume 58, pages 327-346. Vieweg Verlag, 1997.
2. October issue of Flyer, 1997.
3. 26 October – 1 November issue of Flight International, 1994.
4. I. Mary and P. Sagaut. Large Eddy Simulation of flow around an airfoil near stall. *AIAA Journal*, 40(6):1139-1145, 2002.
5. L. Davidson and B. Farhanieh. CALC-BFC: A finite-volume code employing collocated variable arrangement and Cartesian velocity components for computation of fluid flow and heat transfer in complex three-dimensional geometries. Rept. 95/11, Dept. of Thermo and Fluid Dynamics, Chalmers University of Technology, Gothenburg, 1995.
6. P. R. Spalart. Strategies for turbulence modelling and simulations. *Int. J. Heat and Fluid Flow*, 21:252-263, 2000.
7. S. Dahlström. Large Eddy Simulation of the Flow around a High-Lift Airfoil. PhD thesis, Dept. of Thermo and Fluid Dynamics, Chalmers University of Technology, Gothenburg, 2003.
8. P.R. Spalart, W-H. Jou, M. Strelets, and S.R. Allmaras. Comments on the feasibility of LES for wings, and on a hybrid RANS/LES approach. 1st AFOSR Int. Conf. On DNS/LES, Aud. 4-8, 1997, Ruston, LA. In *Advances in DNS/LES*, C. Liu & Z. Liu Eds., Greyden Press, Columbus, OH, 1997.



# Modeling of Time-dependent 3D Weld Pool Due to a Moving Arc

Minh Do-Quang and Gustav Amberg

Mechanics Department, Royal Institute of Technology (KTH), Stockholm

It is well recognized that the fluid flow is an important factor in overall heat and mass transfer in molten pools during arc welding, affecting geometry of the pool and temperature distribution in the pool and in the heat affected zone. These in turn influence solidification behavior, which determine the mechanical properties and quality of the weld fusion zone.

Here, a comprehensive numerical model of the time dependent weld pool flow in gas tungsten arc (GTA) welding, with a moving heat source has been developed. This model included heat transfer, radiation, evaporation, electromagnetic forces and Marangoni stress in the free surface boundary. With this 3D, fully time dependent model, the true chaotic time dependent melt flow is obtained.

The time dependent properties of flow velocities and temperature of numerical results are examined. It shows that the temperature fields are strongly affected by convection at the weld pool surfaces. The fluid flow in the weld pool is highly complex and it influences the weld pool's depth and width. Moreover, the velocity field at the surface of the specimen determines the streamlines defining the traveling paths of inclusions such as slag particles.

## Introduction

Traditionally, in modeling welding phenomena there has been a focus either on the complex fluid and thermo-dynamics local to the weld pool, or the global thermo-mechanical behavior of the weld structure. A variety of simplified models is now frequently employed in the simulation of welding processes, but they are totally reliant on the accuracy of model parameters which describe the weld pool's size and shape. For gas tungsten arc (GTA) welding, the complex fluid flow in the weld pool is mainly driven by forces due to surface tension gradients, electromagnetic, buoyancy, arc pressure and aerodynamic drag force arising from the shielding gas used in GTA welding.

The main restriction in 3D GTA welding simulation is the need for a sufficiently resolved grid, combined with the variety of physical mechanism present in the welding process. It also leads to a consideration of computational time limits. Even if the roles of various physical processes are understood in principle in two dimensions, there is some uncertainty in three dimensions, [16] e.g. some works focus on

the influence of mass, momentum, and heat transfer on weld pool geometry [5, 11, 12, 13]. In those works, the fluid flow is considered as a laminar flow, while others considered the fluid flow as turbulent [4, 6, 10]. In several cases, the turbulent flow in the weld pool has been taken into account by enhancing both the viscosity and thermal conductivity [8, 9, 10]. More recently, DebRoy and coworkers [15, 14, 18] have also used the  $k - \epsilon$  turbulence model in order to model the fluid flow in the weld pool.

There is little direct experimental evidence that suggests whether fluid flow in a weld pool is laminar, turbulent, or transitional. It has been estimated that the Reynolds number varies from 1400 to 3000 [6] and up to 10000 [12]. On the other hand, neither the characteristic length scale most appropriate for determining the Reynolds number for a weld pool nor the critical Reynolds number for the transition from laminar to turbulent flow in a closed cavity flow such as in a weld pool have yet been established, so arguments concerning whether the flow is laminar or turbulent as based on a criterion for a critical Reynolds number are highly tenuous and indeed not valid yet. The physical dimensions of a weld pool are typically of the order of a few millimeters and the flow velocities in the weld pool can reach 1 *m/s* or more. Hence, fluctuating velocities are inevitable when strong recirculating fluid flow occurs in a relatively small weld pool.

The aim of this work is therefore to develop a comprehensive numerical thermo-fluids model of a moving heat source, time dependent, three dimensions GTA welding which included heat transfer, radiation, evaporation, electromagnetic force and viscous stress in free surface boundary conditions. Moreover, fluctuating velocities and temperature are taken into account.

## Modeling approach

### Mathematical modeling

The governing transport equations are transformed into a coordinate system attached to the arc, which travels along the  $y$  direction at a constant speed  $U_s$ . The melt is treated as an incompressible Boussinesq liquid.

$$\nabla \cdot \vec{u} = 0 \quad (1)$$

$$\frac{\partial \vec{u}}{\partial t} + (\vec{u} \cdot \nabla) \vec{u} = -\frac{1}{\rho} \nabla p + \nu \nabla^2 \vec{u} + \vec{S} + \frac{\partial}{\partial y} (U_s \vec{u}) \quad (2)$$

where  $\vec{u}$  is the fluid velocity;  $p$  is the pressure, and  $\vec{S}$  is the source term.

$$\mathbf{S} = \frac{1}{\rho}(\mathbf{J} \times \mathbf{B}) + \frac{\nu}{H(\chi)}\chi\mathbf{u} + \mathbf{g}\beta(T - T_{ref}) \quad (3)$$

The  $\mathbf{J} \times \mathbf{B}$  terms are the Lorentz force components in the respective directions, where the solenoidal vectors  $\mathbf{J}$  and  $\mathbf{B}$  are the current density vector and magnetic flux vector. Those are calculated by solving the Maxwell's equations of the electromagnetic field in the domain of the workpiece. If the effect of fluid motion on the electromagnetic field is neglected, the Lorentz forces are assumed constant and they are computed numerically and included to the system equations as a known body force.

The second terms represent the porous medium model at the solid-liquid interface.  $\chi$  is the fraction of volume occupied by melt,  $\chi$  has a value of 0 in the solid region, 1 in the completely molten region.  $H(\chi)$  is the permeability of the mush [2].  $H(\chi)$  is infinite in the molten region and very rapidly decreases to very small values (say,  $10^{-8}$ ) in the solid region, so that the velocity  $\vec{u}$  will become effectively zero in the solid region.

The additional source term  $\mathbf{S}_z$  in (3) also includes the natural convection within the weld pool:  $g\beta(T - T_{ref})$ , where the Boussinesq approximation has been used.  $\beta$  is the volumetric expansion coefficient of welded material,  $g$  is the gravity acceleration, whereas  $T_{ref}$  is reference temperature (288 K).

Assuming the material change directly from solid to liquid, we can neglect the presence of a mushy-zone. The fraction of volume occupied by solid can be computed, according to [2],

$$\frac{\partial\chi}{\partial t} = \frac{1}{\kappa}(T - T_{liq}) \quad (4)$$

This equation allows a simple way of determining the solid fraction  $\chi$  at the new time level by using the discretized form of the left-hand side: If  $\chi$  tends to increase beyond 1 or decrease below 0, the new value of  $\chi$  is taken to be 1 or 0, respectively. This means that  $T$  is then allowed to differ from  $T_{liq}$ , which, of course, is quite correct in the solid ( $\chi = 0$ ) or the liquid ( $\chi = 1$ ) region. The numerical parameter  $\kappa$  is a small constant, used to amplify any deviation of  $T$  from  $T_{liq}$  and results in a rapid melting or freezing that restores  $T$  to  $T_{liq}$ .

The energy conservation is expressed as follows:

$$\frac{\partial T}{\partial t} + (\vec{u} \cdot \nabla)T - \frac{\partial(U_s T)}{\partial y} = \alpha\Delta T + \frac{L^*}{\rho C_p} \left( \frac{\partial\chi}{\partial t} - \frac{\partial(U_s\chi)}{\partial y} \right) \quad (5)$$

where  $\alpha$  is the thermal diffusivity,  $C_p$  is the specific heat and  $L^*$  is the latent heat of fusion. The two terms containing  $U_s$  appear as a result of the coordinate transformation.

### Numerical modeling

The numerical simulations of weld pool heat and fluid flow were carried out using the *femLego* [1] tool to create a set of C and Fortran code from mathematical equations which were written in Maple format. The model in this project can simulate the physical phenomena mentioned above, such as surface tension gradients, electromagnetic, buoyancy, etc., in the weld pool with moving heat source.

The solution of whole set of equations (1) - (5) can be described as follows: With a given temperature at the previous time level, the phase of the material  $\chi$  (liquid or solid) is computed using equation (4). From the new solid fraction value, the amount of released latent heat of fusion in the energy equation is computed and the temperature can then be obtained at the new time level. Using the new temperature and solid fraction, a pressure and velocity field is obtained from equation (1) and (2). Now all unknowns have been computed at the new time level and the entire procedure restarts.

The equations have been discretized using a finite element approach on an unstructured grid. The type of elements which are used for both velocity, pressure and temperature variables are piecewise linear tetrahedral elements. The restrictions imposed by Babuska-Brezzi condition are avoided by adding a pressure stabilization term. The pressure and velocity solutions are split using a fractional step algorithm. The Poisson equation for the pressure is solved using the well-known Conjugate-Gradient method. The convective term in equation (2) and (5) are calculated implicitly using the GMRES method. In this way a reasonably large time step can be used in the computations. In order to add stability without losing any accuracy we also used a streamline-diffusion method for the convection terms in equations (2) and (5). The spatial derivatives used guarantee a second-order accuracy.

To determine the overall stability of the numerical scheme we introduced a Courant number

$$Co = u_{max} \frac{dt}{dx} \quad (6)$$

where  $u_{max}$  is the maximum velocity in the x-direction in the domain and  $dx$  is the spatial step size. With the present semi-implicit treatment of convective terms, a practical value of Courant number should not increase above a critical value of 2.5. Here, minimum grid space was 0.02 mm and maximum velocity can

reach up to  $1 \text{ ms}^{-1}$ . Hence, the maximum time step that can be applied in this case is  $5 \times 10^{-5} \text{ s}$ .

### Parallel computation

A new parallel version of *femLego*, a finite-element tool for partial differential equations, [3] was developed within the scope of this project. The code is implemented using MPI and achieves parallelism by spatially decomposing the problem into an unstructured collection of structured blocks. The algorithm yields excellent scaling on both the shared memory and distributed memory architecture machines, with the latter yielding a performance improvement factor approximately linear with the numbers of processors used. See Table 1.

Once a distributed matrix is created, the stiffness matrix  $A$  and r.h.s. vector  $b$  are computed locally on each processor. Here, the matrix  $A$  is already partitioned into blocks of rows, with each block assigned to one processor. The associated components of unknowns and r.h.s. vectors are distributed accordingly. Communication may be needed to transfer some components of  $x$ . For example, in  $y \leftarrow Ax$ , if  $y_i$  is update on processor  $p_1$ ,  $A_{ij} \neq 0$ , and  $x_j$  is owned by processor  $p_2$ , then  $p_2$  must send  $x_j$  to  $p_1$ . In general, a processor may need more than one  $x$  component from another processor. The number of components that must be updated is minimized by using the option Fill-reducing reordering that is provided by Metis.

Table 1 shows the calculation times spent on an IBM-SP2 machine and a PC-cluster. Clearly, the speed-up is quite acceptable on the expensive machine (IBM-SP2) and also on the cheapest one, PC-cluster.

CPUs	SP2 machine			PC-cluster		
	Time (s)	Speed-up	Efficiency	Time (s)	Speed-up	Efficiency
1	9800.37	1.0000	100.00%	14660.3	1.0000	100.00%
2	5000.88	1.9597	97.99%	7346.3	1.9956	99.78%
4	2816.38	3.4798	86.99%	3848.6	3.8092	95.23%
8	1236.00	7.9291	99.11%	1955.9	7.4952	93.69%
12	937.09	10.4583	87.15%	1472.1	9.9585	82.99%
15	824.50	11.8864	79.24%			

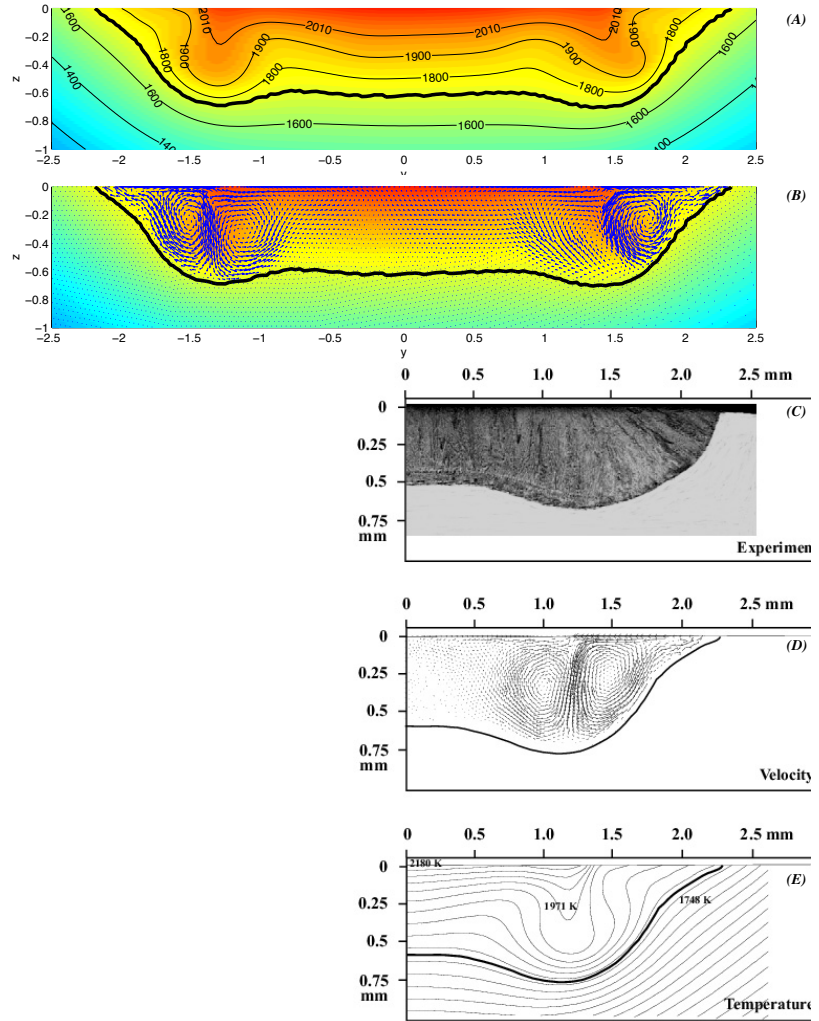
Table 1  
Performance and speed-up of parallel computing

## Results and discussion

### 3D simulation of the welding pool with a stationary arc

Figure 1

AP1-100A: Comparison of experimental and 2D, 3D numerical results after 1 second, (C)-(E) from [12]



In order to validate the code, a three dimensional simulation of welding pool with stationary heat source is carried out. The material is stainless steel type 304 (AP1) which has an extra-low sulfur (0.0005%). The welding current is 100A, arc voltage 10.6V. In comparison with 2D and experimental results (from [12], (C), (D) and (E)), a quite good qualitative and quantitative agreement in the weld pool shapes

can be observed in 3D solutions after 1s (Figure 1 (A), (B)). In the 3D simulation, the weld pool radius and depth became 2.3 mm and 0.6 mm, by comparison with the 2D simulation results of 2.07 and 0.58 and experimental results for radius and depth, 2.25 and 0.52, respectively, show a very good agreement.

As being shown in the previous research, there was an inward motion in the 3D weld pool, that drove the fluid flows in a weld pool and created two vortices in opposite directions. They deepened the groove at the periphery even more than in the center. This occurs for a material which has low sulfur only, when the sign of temperature coefficient of surface tension ( $\frac{\partial\gamma}{\partial T}$ ) would be changed at low temperature, around 1800 K – 2000 K.

The other numerical result for a high content of the surface active element sulfur in the base material (0.0139%) is shown on figure 2D. In this case, we obtained almost the same conclusions about the depth, width and shape of the weld pool with the previous works [12] and [17]. But the fluid flows in this case became much more complex since it seemed to be unstable at the center of the weld pool. This causes the flow to become asymmetric.

### Effect of moving heat source speed

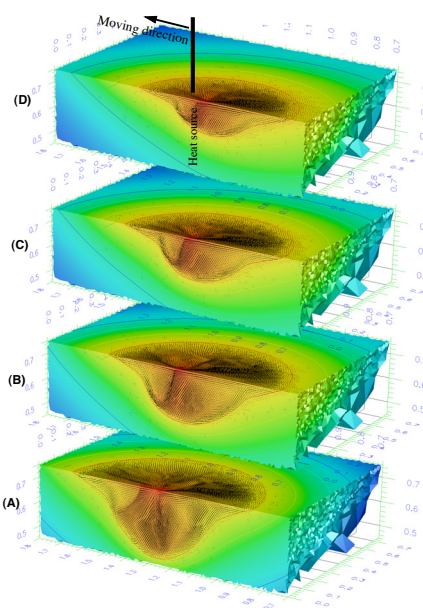
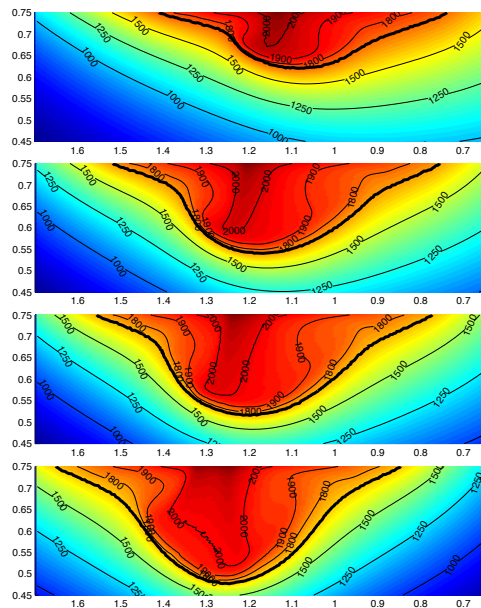


Figure 2  
AP5-100A: Temperature and velocities fields of welding pool.  
 $U_s = 0 \text{ mm} \cdot \text{s}^{-1}$  (A);  $3 \text{ mm} \cdot \text{s}^{-1}$  (B);  $6 \text{ mm} \cdot \text{s}^{-1}$  (C) and  $9 \text{ mm} \cdot \text{s}^{-1}$  (D)

Figure 2 shows the temperature and velocity distributions for 3D GTA welding simulations. The electrode (at position  $y = 1.25$ ) is moving from right to left with a constant speed:  $U_s = 0 \text{ mm} \cdot \text{s}^{-1}$  (A);  $3 \text{ mm} \cdot \text{s}^{-1}$  (B);  $6 \text{ mm} \cdot \text{s}^{-1}$  (C) and  $9 \text{ mm} \cdot \text{s}^{-1}$  (D) respectively. The material is stainless steel type 304 (AP5) with a high sulfur 0.0139%. GTA conditions are:  $I = 100 \text{ A}$ ,  $U = 10.6 \text{ V}$ . The isotherms are shown on the upper surface of the plate and on the vertical symmetry plane oriented along the traveling direction of the electrode. In this case, there is only one motion toward the center of the pool, since the temperature that is needed to change the sign of the coefficient of surface tension is  $2300 \text{ K}$ , greater than the maximum temperature of the weld pool.

It is observed that the temperature fields are strongly affected by convection, at the weld pool surfaces. The fluid flows in the weld pool are highly complex and these influence the weld pool's depth and width. When the heat source is moving, the volume of the weld pool is decreasing and the centroid of the weld pool is moving along behind the arc. Moreover, the velocity field at the surface of the specimen determines the streamlines defining the traveling paths of inclusions such as slag particles.

An overview of the numerical results for the weld pool with moving heat source on stainless steel type 304 can be found in Table 2.

Table 2  
Summary of numerical results and effective of moving heat source

Moving speed ( $\text{mm} \cdot \text{s}^{-1}$ )	$U_{max}$ ( $\text{m} \cdot \text{s}^{-1}$ )	$T_{max}$ (K)	pool width (mm)	pool depth (mm)
0	0.9394	2193	3.9808	1.3589
3	0.9214	2170	3.7806	0.9324
6	0.9166	2115	3.6150	0.8354
9	0.9085	2099	2.9778	0.5581

### Time dependent

The simulation of a weld pool with a stationary heat source is used to study the time dependent problem. The material is high sulfur content (0.0139%) stainless steel (AP5-100A). The welding conditions are the same as in the previous sections.

The evolution of temperature of three testing points is shown in Figure 3. The three positions of testing points are defined at the centerline in the  $z$  direction of the weld pool. It is observed that the weld pool is fully developed after  $1 \text{ s}$  and the

temperatures at three testing points are time dependent. The highest amplitude of temperature fluctuations is 50 K at the top point and 25 K for the bottom point. The highest temperature in the weld pool is less than 2300 K, the critical temperature in order to change the sign of temperature coefficient of surface tension ( $\frac{\partial \gamma}{\partial T}$ ). Therefore, there is only one vortex in the pool.

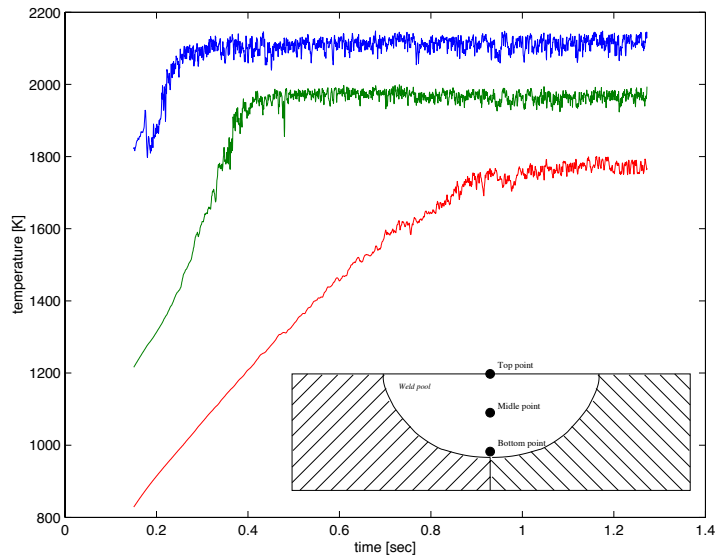


Figure 3  
The temperature evolution of three testing points

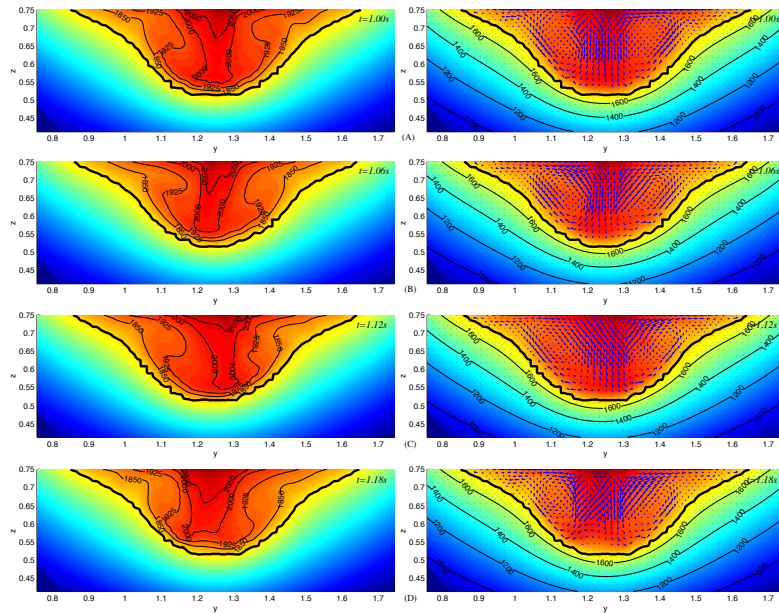


Figure 4  
3D simulation, temperature distribution and velocity field time dependent

The temperature distribution and velocity field at the symmetry plane  $x = 0$  at the different times  $t = 1.0 \text{ s}$ ,  $t = 1.06 \text{ s}$ ,  $t = 1.12 \text{ s}$  and  $t = 1.18 \text{ s}$  are shown in figure 4. The flow fields are in general quite complex and highly time dependent (chaotic), as is visible in all plots. The physical dimension of this weld pool is approximately  $4 \text{ mm}$ , the flow velocities in the weld pool can reach  $1 \text{ ms}^{-1}$  and the kinematic viscosity of the steel  $\nu = 6.81 \times 10^{-7} \text{ m}^2\text{s}^{-1}$ . Hence, the Reynolds number is  $Re \approx 5800$ . At the center of the weld pool, below the arc position, the flow velocity is maximum ( $\approx 1 \text{ ms}^{-1}$ ) and there is an instability flow which occurred by a radially inward flows on the free surface. The area of the liquid that has  $T > 2000 \text{ K}$  looks like a column at the center of the pool and is obviously unstable. It swings to left then right at the different times. See figures (4A, 4B, 4C, 4D). The depth, width and even the shape of the weld pool remain the same during the study, even through some small oscillation is present here to.

There are two big vortex rings in figure 4 that appeared almost in the whole weld pool. They keep the shape of the pool remains unchanged; even the fluid flows of the pool at the center are unstable. Otherwise, when a strong recirculating fluid flow occurs in a relatively small weld pool such as this fluctuating velocities are inevitable. This can be a reason for the appearance of the highly time dependent (chaotic) flow in the weld pool.

## Conclusions

It has been shown successfully that it is possible to simulate GTA welding in three dimensions by using the *femLego* tool, a numerical simulation tool by symbolic computation.

The present 3D modeling study shows that the welding speed may affect the melt flow and temperature distribution in GTA welding. The melt flow field predicted by the present 3D modeling is much more complex than that obtained from the previous 2D modeling.

We first show the highly time dependent (chaotic) problem in GTA welding. This appears when a strong recirculating fluid flow occurs in a small weld pool. A systematic research of the properties of this time dependence needs further study.

## References

- [1] Numerical simulation by symbolic computation. <http://www.mech.kth.se/~gustava/femLego>.
- [2] G. Amberg. Computation of macrosegregation in an iron-carbon cast. *Int. J. Heat Mass Transfer*, 34(1):17-227, 1991.
- [3] G. Amberg, R. Tönhardt, and C. Winkler. Finite element simulations using symbolic computing. *Mathematics and Computers in Simulation*, 49:149-165, 1999.
- [4] R.T.C. Choo and J. Szekely. The possible role of turbulence in gas weldpool behavior. *Weld J.*, 73(2): 25s-31s, 1994.
- [5] T. DebRoy. Mathematical modeling of fluid flow and heat transfer in gas metal arc welding. *Mathematical Modeling of Weld Phenomena*, 5:1-31, 2001.
- [6] K. Hong, D.C. Weckman, A.B. Strong, and W. Zheng. Modelling turbulent thermofluid flow in stationary gas tungsten arc weld pools. *Sci. Technol. Weld. Joi.*, 7(3):125-136, 2002.
- [7] C.S. Kim. Thermophysical properties of stainless steels. Technical report, Argonne National Laboratory, 1975.
- [8] K. Mundra, J.M. Blackburn, and T. DebRoy. Absorption and transport of hydrogen during gma welding of low alloy steel. *Sci. Technol. Weld. Joi.*, 2(4): 174-184, 1997.
- [9] K. Mundra, T. DebRoy, and K.M. Kelkar. Numerical prediction of fluid flow and heat transfer in welding with a moving heat source. *Numer. Heat Tr. A*, 29(2): 115-129, Feb. 1996.
- [10] T.A Palmer and T. DebRoy. Numerical modeling of enhanced nitrogen dissolution during gas metal arc welding. *Metall. Mater. Trans. B*, 31B:1371-1385, 2000.
- [11] M. Ushio and C.S. Wu. Mathematical modeling of three-dimensional heat and fluid flow in a moving gas metal arc weld pool. *Metall. Mater. Trans. B*, 28B: 509-516, June 1997.
- [12] C. Winkler, G. Amberg, H. Inoue, and T. Koseki. A numerical and experimental investigation of qualitatively different weld pool shapes. *Mathematical Modelling of Weld Phenomena 4*, pages 37-69, 1998.
- [13] T. Xacharia, A.H. Eraslan, D.K Aidun, and S.A. David. Three-dimensional transient model for arc welding process. *Metall. Trans. B*, 20B:645-659, 1989.
- [14] Z. Yang and T. DebRoy. Modeling macro-and microstructures of gas-metal-arc welded hsla-100 steel. *Metall. Mater. Trans. B*, 30(3):483-493, Jun. 1999.
- [15] Z. Yang, J.W. Elmer, J. Wong, and T. DebRoy. Evolution of titanium arc weldment macro and microstructures - modeling and real time mapping of phases. *Weld J.*, 79(4):97S-112S, Apr. 2000.

- [16] X. H. Ye and X. Chen. Three-dimensional modelling of heat transfer and fluid flow in laser full-penetration welding. *J. Phys. D: Appl. Phys.*, 35:1046-1056, 2002.
- [17] T. Zacharia, S.D. David, J.M. Vitek, and T. Debroy. Weld pool development during gta and laser beam welding of type 304 stainless steel, part ii - experimental correlation. *Welding Journal Research Supplement*, 68:510s-519s, 1989.
- [18] H. Zhao and T. DebRoy. Weld metal composition change during conduction mode laser welding of aluminum alloy 5182. *Metall. Mater. Trans. B*, 32(1):163-172, Feb. 2001.

# Virtual-Reality Environment for Visualization of Unsteady Three-Dimensional CFD Data

Stefan Görtz and Elias Sundström

Department of Aeronautical and Vehicle Engineering, Royal Institute of Technology (KTH), Stockholm

A Virtual-Reality (VR) environment has been set up at PDC to visualize, explore and interact with pre-calculated steady and time-dependent three-dimensional CFD solutions in a fully immersive way. This report presents the VR system and provides some examples of currently investigated applications in the area of computational aerodynamics.

## Introduction

Large-scale simulations of three-dimensional, time-dependent flow fields are now commonplace in state-of-the-art computational fluid dynamics (CFD). Such numerical simulations produce large amounts of flow-field data, often with several thousands of discrete time steps. Each time step may require tens or hundreds of megabytes of disk storage, and the entire data set may be hundreds of gigabytes [1, 2]. Fluid flow features such as boundary layers, separation, recirculation bubbles, shocks, multiple vortices and vortex breakdown are items of interest that can be found in the computed results. However, analyzing, visualizing and communicating these unsteady three-dimensional CFD results in 2D visualization environments is inherently difficult because of perceptual problems such as occlusion, visual complexity, lack of directional cues, and lack of depth cues. This has resulted in a rapidly growing need for 3D visualization tools. The computer system requirements for such tools are substantial. They include speed of computation, ability to quickly render high-resolution graphics, and massive data storage and retrieval capabilities [2]. At PDC such a tool is available with the virtual-reality (VR) cube.

## The PDC virtual-reality cube

The VR cube at PDC is a fully immersive visualization environment. Its unique feature is the display of images on all surrounding surfaces, including the floor and the ceiling. The six displays are synchronized to provide the users with a single surrounding 3D view. The display system is based on high-resolution back-projection that provides stereoscopic images when viewed with lightweight 3D LCD shutter glasses. A 3D input device or a glove is used to manipulate the objects and interactively interrogate the data.

Several persons can enter and walk freely inside the VR cube and see 3D images

together. The main advantage over ordinary graphics systems is that the viewers are surrounded by the projected images, which means that the images are the users' main field of vision. This surround view adds to the immersion, as the peripheral vision is an important part of the human orientation capabilities [1]. A head tracking system continuously adjusts the stereo projection to the current position of the leading viewer so that what is displayed preserves proper perspective in adapting to movements and change of location of gaze. That is, perceptually, the user sees the virtual scene in a manner consistent with if it were real. The objects in the virtual scene do not just appear on the walls of the VR cube and beyond. They can appear to enter into the physical space of the VR cube itself, where the user can interact with them directly. It is easy to mix real and virtual objects in the same environment. The viewers can for example see their own hands and feet as part of the virtual world. This gives them a heightened sense of being inside that virtual world.

The visualization software used with the VR cube is the COVISE software [3], a modular visualization software supporting VR for multi-sided projection, tracking and collaborative working in networks. A head-up macro within the software provides user interface panels on the display that can be used to change the viewing scene or attributes of models in the screen. Standard post-processing tools such as streamlines, pathlines, streaklines, iso-surfaces and particle animation are available. These are computational analogues of the classical wind-tunnel techniques such as smoke injection, dye advection, time-exposure photographs, tufts, etc. [2].

## Applications

In the following, we describe the visualization of three cases in the VR cube. The first scenario, the flow over a delta wing, was the original motivation to go into the VR cube. For this reason, this case is presented in greater detail than the other two cases.

### Case Study I: Vortex breakdown over full-span delta wing

The first case study deals with the inherently unsteady flow field over a stationary  $70^\circ$  full-span delta wing at an angle of attack of  $\alpha = 30^\circ$ ,  $M_\infty = 0.2$ . At this angle of attack vortex breakdown occurs. Inviscid, time-accurate calculations were performed with the compressible Navier-Stokes multi block (NSMB) solver, using explicit global Runge-Kutta time stepping and a structured grid with 1,674,752 cells. This work and the flow solver are described in more detail in [4, 5]. Here, we focus on demonstrating the benefits of visualizing this complex flow in the VR cube. A standard technique for analyzing a vortical flow field is to look at the spatial and temporal development of vortex cores. Vortex cores are at the center of swirling flow. Vortex cores reveal vortex burst, which is characterized by a sharp kink in the vortex core filament. By releasing e.g. pathlines,

streaklines and animated particles into the computed flow field, the viewer can explore physical phenomena such as oscillations in the vortex breakdown location, or asymmetric vortex breakdown. For this purpose, a COVISE network with looping properties was created in order to load and animate 60 of the more than 1,500 time steps that were saved to disk. The network was configured to allow for setting interactive cutting planes, placing iso-surfaces and initiating particle traces from inside the VR cube. Data reduction modules were used to load as many time steps as possible into the main memory.

Streaklines belong to the class of time-dependent flow visualization techniques which are based on many instants of the flow fields in time. A streakline is a curve formed by all particles that were previously injected from a fixed location. Streaklines are effective visualization techniques for depicting vortex shedding and vortex breakdown in unsteady flows [6]. Figure 1 shows numerical streaklines colored by velocity magnitude at six different time steps. Numerical streaklines are represented as discrete points, because particles are injected at discrete time steps. The time resolution of the numerical flow dictates how continuous the streaklines appear. For reasons of disk space, most large-scale 3D unsteady flow simulations are sampled at a coarse time resolution, for example, at every 50th or 100th time step. Hence, numerical streaklines may not always be smooth. The time resolution of the data used here, however, is good enough to reveal the basic flow-field features. Note that the placement of the seed points of the streaklines can be critical in obtaining a good depiction of the flow. Here, the streaklines appear to show spiral-type vortex breakdown, where the vortex core filament abruptly kinks and starts to spiral around the axis of the structure, forming a corkscrew-like distortion of the vortex core. Furthermore, the rotation of the port and starboard post-breakdown helical structures is seen to be slightly out of phase.

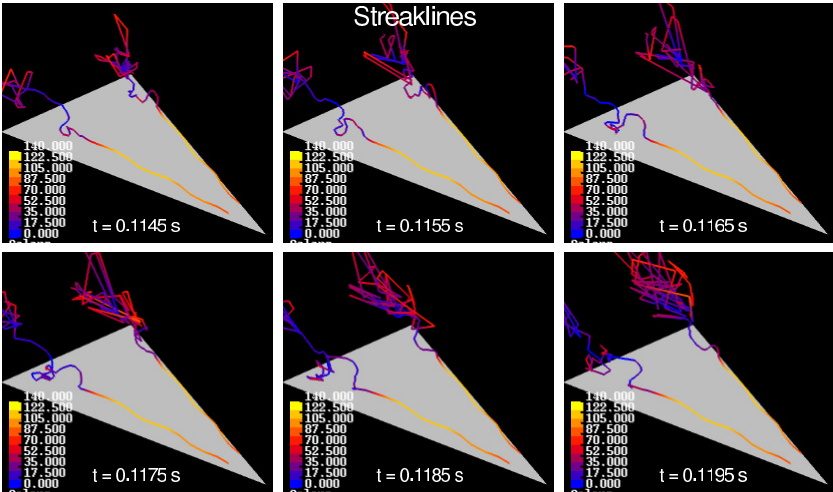
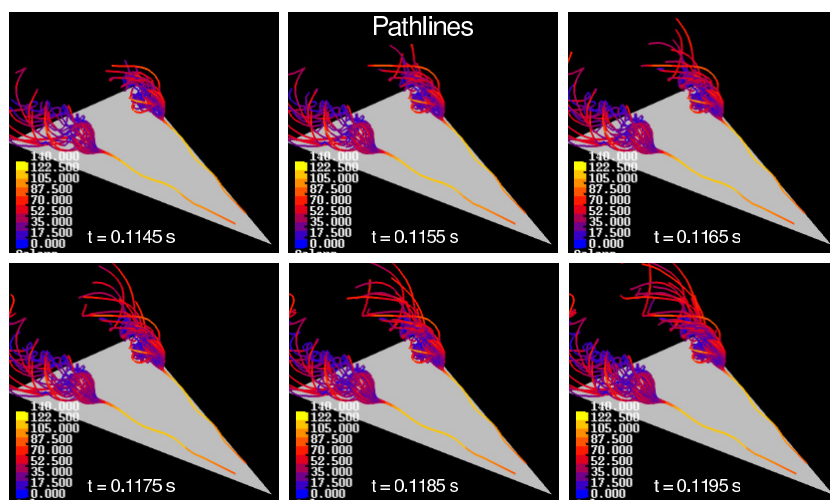


Figure 1  
Snapshots of time-dependent streaklines at different times colored by velocity magnitude.

Figure 2 shows pathlines at six different time steps. The pathlines are colored by velocity magnitude. Four pathlines are released in the same way as the streamlines for each time step. When the pathlines reach the breakdown zone, the structure of the vortex breakdown becomes vague. In contrast to the moving points it appears that a bubble type vortex breakdown is present. The bubble-type mode is characterized by a stagnation point on the vortex axis followed by an oval-shaped recirculation zone, with the core flow spreading out symmetrically at the stagnation point and passing smoothly around the recirculation zone.

Figure 2  
Snapshots of time-dependent pathlines at different times colored by velocity magnitude



Clearly, the appearance of the structure of vortex breakdown depends on the visualization method used. With streaklines and moving points the broken down vortex core resembles a spiral, whereas it looks like a bubble when visualized with pathlines.

Figure 3 shows six snapshots of a pressure-coefficient iso-surfaces,  $C_p = 0.28$ . The time interval between snapshots is 0.001 s and about one full rotation of the spiral structure downstream of the breakdown point can be seen. The period of rotation is approximately  $T = 0.008$  seconds, which is in good agreement with experimental data for this test case, compare the more detailed results in [4, 5]. This rotation of the helical vortex structure in the breakdown region causes oscillations of the surface pressure coefficient, which cause oscillations in the aerodynamics coefficients. A close look at the iso-surfaces in Figure 3 also reveals that the starboard vortex is out of phase relative to the port-side one.

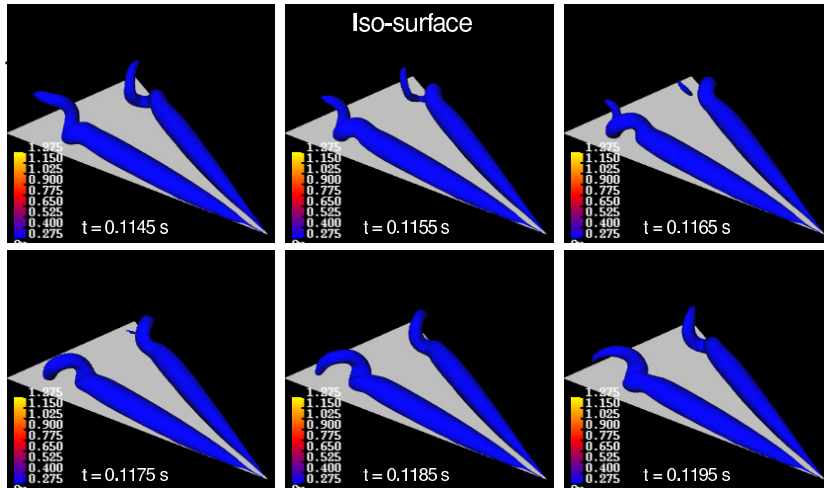


Figure 3  
Snapshots of pressure coefficient iso-surfaces at different times.

This lead-lag effect is even more visible in Figure 4, which shows iso-lines and a cutting plane colored by  $C_p$ . Here, the iso-value separation is set to  $\Delta C_p = 0.02$ . Clearly, the numerical solution exhibit asymmetry despite symmetric boundary conditions and a symmetric grid. The influence of the helical structure on the upper surface can clearly be seen. Regions of low pressure are generated where the helix comes in proximity with the surface. These regions of low pressure are seen to form upstream near the initial breakdown location and move downstream with the progression of the rotating helical structure. This leads to fluctuations in the aerodynamic coefficients.

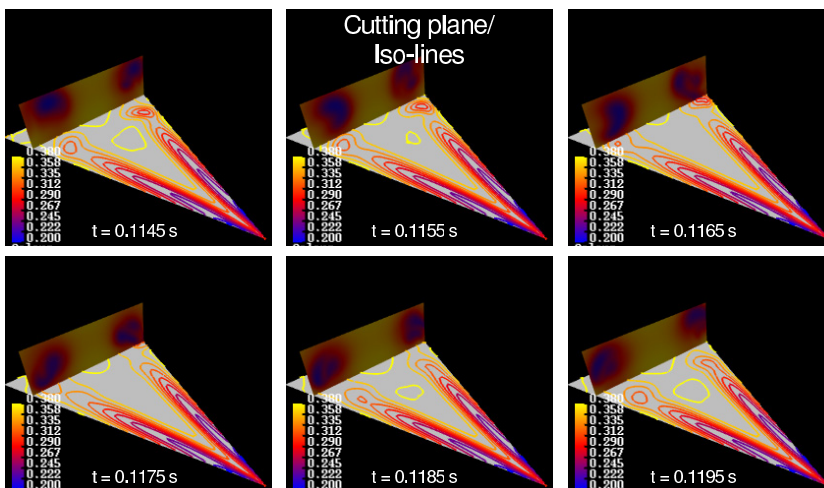


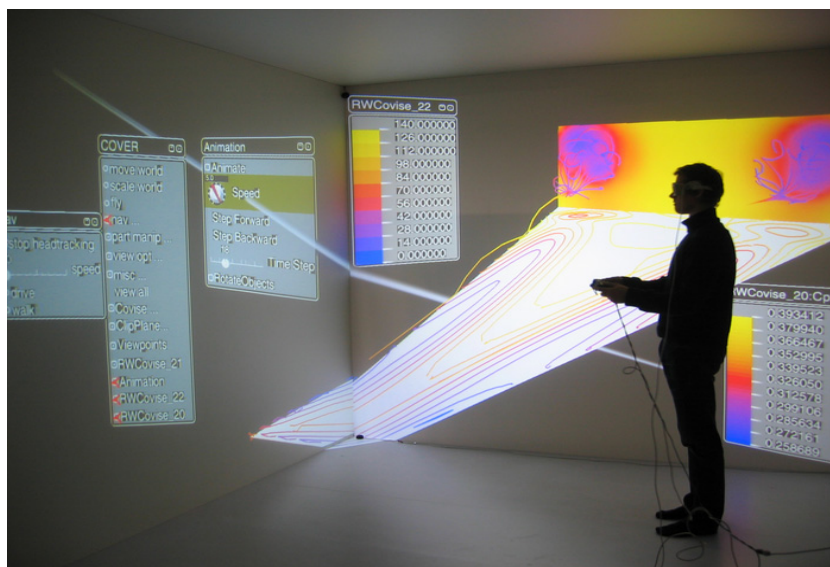
Figure 4  
Snapshots of  $C_p$  isolines and cutting surface colored by pressure coefficient.

Note that the static 2D pictures in this paper can by no means convey the visual sensation in the VR cube. It is very difficult to interpret the unsteady flow over the delta wing using these pictures. For example the spiral rotation of the vortex core in the post-breakdown region is difficult to understand in 2D, but easily grasped in the VR environment. Being able to insert particles into the flow by just releasing them with the 3D input device at the seen position is very natural and allows even people who are not analysis experts to immediately participate in the discussion of the simulated flow.

### Interactive flow-field visualization in the VR cube

Figure 5 shows an interactive visualization session inside the VR cube. For this photograph, animation, head tracking and stereo viewing were switched off, making the display appear non-immersive (otherwise the photograph would be blurred due to the long exposure time). The COVER menu and the animation submenu are shown on the left wall. The delta wing and an instant in time of the corresponding unsteady flow field are projected mainly on the rear wall, together with color bars for the pressure coefficient and velocity magnitude. The flow field is visualized using a cutting plane colored by pressure coefficient, pathlines colored by velocity magnitude and pressure coefficient iso-lines on the wing's surface. Both the cutting plane and the pathlines are controlled interactively. Since the flow is pre-computed, it can be investigated at any length scale, and with control over time, for detailed analysis of long- and short-duration phenomena. In Figure 5 the user is seen changing

Figure 5  
Time-dependant flow over delta wing visualized in the VR cube (stereo mode switched off). Note the virtual "laser beam" pointing at the animation menu to the left. Cutting plane colored by  $C_p$ .



the animation speed by intersecting a virtual “laser beam” extending from the 3D input device with the “speed” entry in the animation menu.

Compared to cheaper “flat screen” visualization methods, the benefit of visualizing the flow field inside the VR cube is that one can “walk around” the delta wing and explore the surrounding flow. When wearing stereo glasses, the delta wing seems to “float” in the middle of the room. The sheer sensual impact of the immersive display has a powerful effect on the physical intuition.

### Case Study II: Atmospheric reentry demonstrator

Next, the hypersonic flow over ESA’s atmospheric reentry demonstrator (ARD) was visualized in the VR cube. The steady-state inviscid flow simulation was performed using the compressible flow solver NSMB as part of a project that dealt with extending the implicit LU-SGS scheme to non-equilibrium reacting flows.

The flow conditions correspond to an altitude of 44 km and a freestream Mach number of  $M_\infty = 10$ . Non-equilibrium reacting flow was assumed. Due to the high Mach number a shock wave forms upstream of the capsule. The shock wave induced heating of the air bathes the heat shield into a hot dissociated gas. The temperature distribution on the heat shield is shown in the visualization in Figure 6. Note that due to the relatively high angle of attack, the temperature is highest on the lower parts of the heat shield, corresponding to the stagnation point.

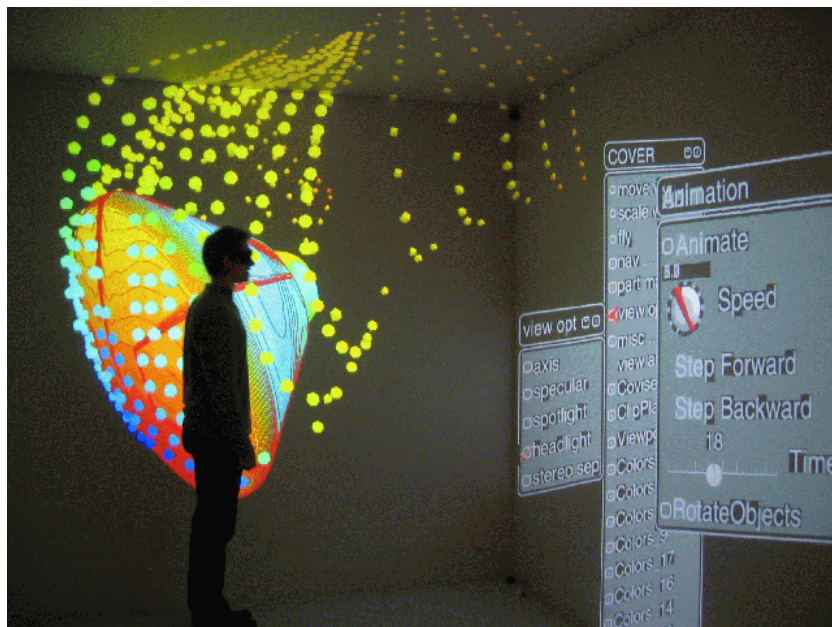
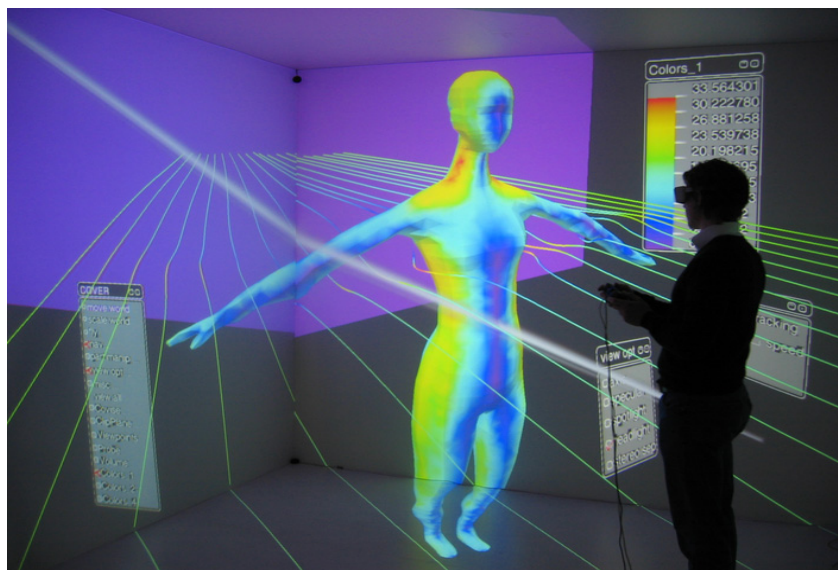


Figure 6  
Hypersonic non-equilibrium reacting flow around ESA’s atmospheric reentry demonstrator (ARD).  
 $M_\infty = 10$ ,  $p_\infty = 165$  Pa,  $T_\infty = 268$  K,  $\alpha = 20^\circ$

The temperature is seen to decrease rapidly around the shoulders of the heat shield due to the expansion of the flow. Note that due to significant non-equilibrium effects on the flow composition around the vehicle, the temperatures are lower than what would be predicted by assuming calorically or thermally perfect gas. Figure 6 also shows animated streamlines colored by velocity magnitude. The particles were released from a plane upstream of the capsule. A subsonic flow region (dark-blue particles) is observed between the shock and the heat shield.

Figure 7  
Airflow around a human female standing in a strong headwind ( $u_\infty = 20$  m/s, ISA sea level)



### Case Study III: Human female standing in strong headwind

Figure 7 visualizes a steady-state Euler solution computed with the unstructured grid flow solver *Edge* [7], simulating the airflow around a human female standing in a strong headwind (uniform 20 m/s, ISA sea level). The images show a “rake” of streamlines and a color mapping of the surface-tangential flow velocity. The solution was obtained using 4-level multigrid, with 20,000 points in the finest grid. The unstructured grid was generated from a public domain IGES geometry (asymmetric) using *ICEM Tetra* and the flow visualization was performed using *COVISE*. This flow simulation, including gridding, was completed in October 2003 by Stephen Conway at the Swedish Defence Research Agency (FOI/FFA), Stockholm.

## Summary

We found that visitors to the VR cube find it exciting and impressive to be able to “walk around” an object and explore the surrounding flow. The sheer sensual impact of the immersive display has a powerful effect on the physical intuition and makes it possible to gain a quick, intuitive understanding of the flow. It is impossible for a “flat screen” display to even come close to this, far less so a set of static 2D pictures in a report. Also, the collaborative environment of the VR cube amplifies the human power for group problem solving and enhances communication.

Clearly, one of the most important applications of the VR cube is in communicating CFD solutions. Unsteady flow phenomena can be demonstrated and explained to people who do not have the interpretive skills needed to interpret “flat screen” displays. This is for example how the VR cube is used in architecture and other design disciplines.

One disadvantage is that the VR cube is a shared resource in a separate building. It has to be booked and data transferred and set up. While this structure can support formal review, presentation and detailed analysis of CFD solutions, it does not lend itself to casual or spontaneous visualization sessions.

## References

1. U. Lang. Present and Future of Visualization applied to Aerospace Engineering. ECCOMAS 2000, September 2000.
2. S. Bryson and C. Levit. The Virtual Windtunnel: An Environment for the Exploration of Three-Dimensional Unsteady Flows. Technical Report RNR-92-013, NASA Ames Research Center, October 1992.
3. D. Rantzau, K. Frank, U. Lang, D. Rainer, and U. Wössner. Covise in the cube: An environment for analyzing large and complex simulation data. In Proc. 2nd Workshop on Immersive Projection Technology (IPT '98), Ames, Iowa, May 1998.
4. S. Görtz. Time-Accurate Euler Simulations of a Full-Span Delta Wing at High Incidence. AIAA Paper 2003-2004, 2003.
5. S. Görtz. Unsteady Euler and Detached-Eddy Simulations of Vortex Breakdown over a Full-Span Delta Wing. ECCOMAS 2004, July 2004.
6. A. D. Lane. Scientific Visualization of Large-scale Unsteady Fluid Flows. AIAA Paper 96-0048, 1996.
7. Swedish Defence Research Agency (FOI), Aeronautics Div. (FFA). Official website for the Edge CFD code. <http://www.edge.foi.se>, accessed 03/2004.



# VirtualFires: A Virtual Reality Simulator for Tunnel Fires

Gernot Beer<sup>1</sup>, Thomas Reichl<sup>1</sup>, Gunther Lenz<sup>1</sup> and Gert Svensson<sup>2</sup>

<sup>1</sup> Institute for Structural Analysis, Graz University of Technology, Austria

<sup>2</sup> Center for Parallel Computers, Royal Institute of Technology (KTH), Stockholm

The VirtualFires (Virtual fire emergency) simulator is presented. It allows training fire fighters in the efficient mitigation of fires in a tunnel and in rescue operations, using a computer generated virtual environment. The simulator can also be used to test the fire safety of a tunnel and the influence of mitigating measures (ventilation, fire suppression etc.) on its fire safety level. The simulator is developed with financial support from the European community under the IST (information society technology) program and combines the simulation of fires using advanced computational fluid dynamics (CFD) software on parallel computers and the visualization of smoke, toxicity levels and temperature with virtual reality (VR).

## Introduction

Past serious fire accidents in tunnels have highlighted the problems that exist with respect to the safety of tunnels and the prevention of serious fatalities in the case of a fire. This required action on a European scale with respect to

- Ascertaining the safety level of existing tunnels and retrofitted tunnels (e.g. the Mont Blanc tunnel).
- The specification of the required safety features and installations for new tunnels.
- Training of rescue personnel in order to increase the efficiency of fire and smoke mitigation procedures.
- Training of drivers with respect to correct behavior in the case of a fire emergency.

With respect to ascertaining the safety level of existing and retrofitted tunnels much reliance is still placed on real tests using fire/smoke pans or vehicles set on fire. Such a test has been recently performed for example in the refurbished Mont Blanc Tunnel. Also fire fighting exercises are usually carried out on a regular basis using burning vehicles or cold smoke generators.

The disadvantages of real tests are that they are expensive, can only be carried out at certain times and are not environmentally friendly since toxic smoke is produced. In a virtual test the tunnel and the fire emergency only exists in computer memory. Using computational fluid dynamics (CFD) computations, the spread of fire and smoke in a particular tunnel is calculated and then visualized.

The tunnel including the safety installations, traffic signs, vehicles etc. is dis-

played together with the results of the CFD calculations using the method of virtual reality. Under the term virtual reality we mean total immersion in a three-dimensional data set. The simulator can be used as a training tool for fire fighters and for assessing the safety level of existing or retrofitted tunnels. It may also be used to check the design of a planned tunnel with respect to ventilation, exits, rescue chambers and other equipment.

The simulator can operate in two modes: One where the CFD simulations are carried out prior to the visualization (pre-calculated scenario) and one where the CFD simulations are carried out concurrent with the visualization. The advantage of the second type is that fire mitigation operations can be performed and that ventilation characteristics may be changed during a session and the resulting effect can be seen immediately (e.g. one may check the effect of reversing the ventilation on the spread of smoke and fire). The first type of system can be used for the training of fire fighters and drivers and for checking the fire safety of existing tunnels. In the first type of system it is possible to pre-calculate several alternatives and the user can select which alternative to choose when the fire is visualized. This is very useful in an educational situation.

### **Visualization Hardware**

The simulator is implemented in a scalable way which means that the visualization can be done on a normal PC, a PC with a head-mounted display (HMD) or in a CAVE environment. A CAVE is a multi-person, room-sized, high-resolution, 3D video and audio environment. Graphics are projected in stereo onto the walls, the floor and the ceiling, and viewed with shutter glasses (see Figure 1). As a viewer wearing a position sensor moves within the display boundaries, the correct perspective and stereo projections of the environment are updated in real time by the rendering system, and the images move with and surround the viewer. Hence stereo projections create 3D images that appear to have a continuous presence both inside and outside the projection room. To the viewer with stereo glasses, the projection screens become transparent and the 3-D image space appears to extend to infinity. Different display-systems have different advantages and disadvantages. A normal PC screen is something everyone has. The images are also normally of good quality but it may be hard to navigate due to the flat appearance. The HMD is portable and lightweight and requires a moderate computing power for image rendering. Only two different images of the scene need to be generated for a given frame rate. The disadvantage is that the user is not fully immersed into the scene due to the limited field of view. The impression is more like watching the scene through the glasses of a diver. Another disadvantage is the low resolution of the display. The CAVE has a wide field of view because the user is fully immersed into the scene

and there is a very high resolution of the rendered scene. The disadvantage is that it is a stationary installation and high computing power is needed for rendering. Depending on the number of projection walls 8 to 12 images are required at the given frame rate.



Figure 1  
User in a CAVE wearing shutter glasses

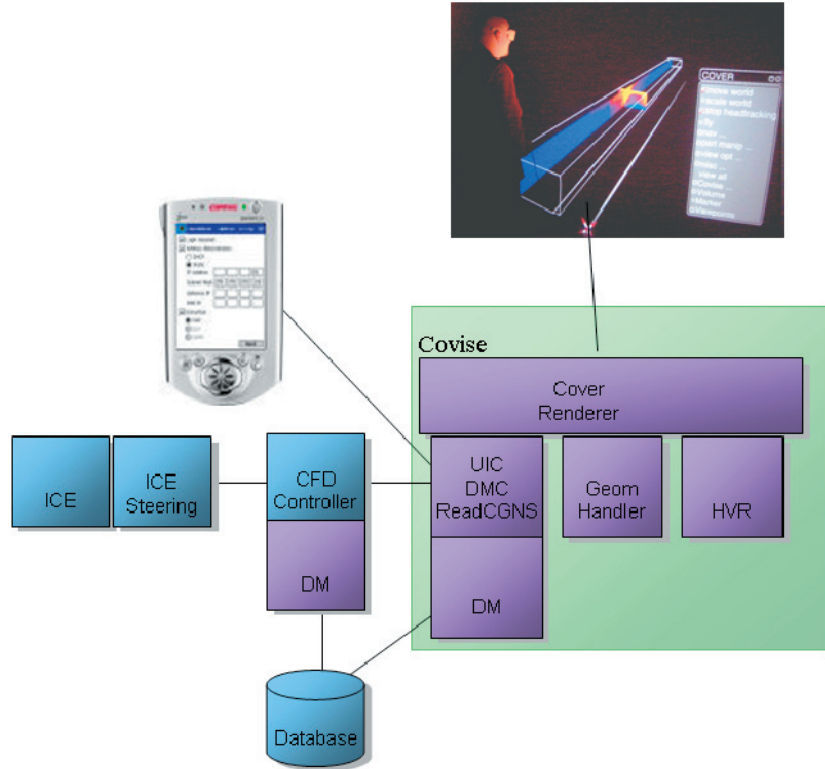
### Software architecture

The layout of the software is depicted in Figure 2. At the heart of the system is the CFD simulation software ICE, which uses the lattice Boltzmann (LB) method [1, 2] to compute the air velocity, temperature, pressure and smoke density at a cell point due to a fire. The “smoke density” is an artificial quantity, which varies between 0 and 1. The smoke production is taken to be proportional to the CO and CO<sub>2</sub> standardized production curves provided as input. It must be pointed out that smoke is a result of fuel rich combustion and the modeling via standardized curves is only a very crude approximation. However, a real combustion model requires input data, which are normally not available and the calculation is very time consuming.

The storage and retrieval of the calculated CFD data and the states of all objects that are involved in a simulation-run is handled by the Database Manager module. This component serves as the communication layer between the simulation front end and the database server back end. Currently it transparently supports the MySQL 4.0.15 open source SQL server, but is adaptable to any other SQL server.

The communication between the CFD solver and the storage layer is done by the data manager controller module. This module has been integrated into the Covise VR environment [3] and also handles all requests from the user interface.

Figure 2  
The VirtualFires software architecture



### Visualization methods

Within the project also some new visualization techniques have been developed. This was necessary as the currently available techniques were not sufficient for the system, mainly for two reasons:

1. They were too slow to handle the amount of the data produced by the CFD to update the rendering in real time
2. They were not capable of rendering photo realistic fire and smoke

These visualization methods were integrated as plug-ins for the Covise [3] renderer Cover and can be managed from the user interface. The photo realistic rendering<sup>1</sup> of smoke is done by a fast volume rendering approach which takes advantage of the availability of programmable shader functions on modern graphics boards. This way frame rates around 25fps for the volume rendering of the CFD results are possible on normal PC hardware. To achieve a photo realistic rendering of fire a fractal 3D texture is applied to the regions of the flames. As CFD results

<sup>1</sup> Photo realistic smoke and fire rendering is currently only available on the Windows platform

are to coarsely spaced compared to the fast visual fluctuations of a flame front, this behavior is interpolated by the fractal texturing process until the availability of the next CFD result. The following scientific visualization methods are currently available on most platforms:

1. Isosurfaces
2. Line integral convolution
3. Streamlines



Figure 3  
Temperature isosurface in a tunnel fire



Figure 4  
"Realistic" visualization of smoke and fire

## CFD simulation

### ICE

The LB method is a recent method for solving fluid flow problems based on kinetic theory. The basic idea is to solve a discretised form of the discrete Boltzmann equation. It can be shown that the solution of the lattice Boltzmann equation is equivalent to the solution of the Navier-Stokes equations within the limit of small Mach numbers. Compared to conventional CFD tools the LB method is in a relatively early, rapidly developing, stage. There are some features, which made us to choose the LB method approach in this project:

- As the LB method works on orthogonal equidistant grids and only involves communication with the next neighbors, parallelization can be done very effectively.
- Time consuming grid generation can be avoided for LB methods by using a simple marker-and-cell approach
- The LB method as an explicit numerical scheme does not require iterations. This in turn means – as long as certain a-priori known stability criteria are taken into account – that divergence problems do not occur and the required computational effort and hence solution time to perform real time simulations can be precisely determined.
- Furthermore due to the simple structure of the algorithm computational programming of the LB method is straightforward.

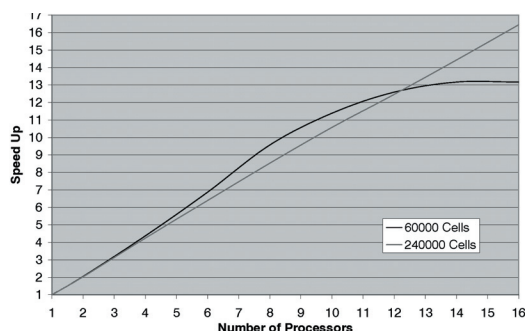
Unfortunately there are also some drawbacks of LB method, see [5].

There were multiple objectives which have been solved during the course of the project and implemented in the ICE code:

- Development and implementation of a flow solver based on the LB method and capable of simulating turbulent buoyant fluid flow problems.
- Implementation and testing of combustion models suitable to simulate compartment and tunnel fires.
- Parallelization of the solver in order to achieve real time simulation capabilities.

The speedup of the parallelization can be found in Figure 5.

Figure 5  
The speed up of ICE for two different sizes of the grid



### 1D – 3D Coupling

The main purpose of a coupling between the 1D and 3D (Figure 6) models is to enable simulation of the smoke and fire development in longer tunnels. The idea of coupling between the two models is based on the attempt to use benefits of both models: the 3D model should be used near the source of fire where the flow is turbulent and the detailed description needed, while the 1D model should be sufficient to describe the flow far from the fire. The use of a simple 1D model makes considerable savings in CPU and memory utilization possible,

Coupled models [4] usually predict the sizes of the 3D and 1D areas in advance and these areas remains unchanged during the simulation. This is a serious drawback for the simulation of smoke development because of the dynamics of the flow. The area where the flow is turbulent, which should be simulated in 3D, varies during the simulation and depends on several factors e.g. fire load, flow velocity, openings and ventilation.

A new coupled model is developed where the 3D and 1D areas (i.e. grids) vary during the simulation. The areas can be expanded or reduced in both directions which depend on the state of the flow at the boundaries between the areas. In this model, the turbulent flow is well captured within the 3D area during the simulation. On the other hand, the flow in the 1D area remains "one-dimensional", which is necessary for the 1D model to be well-defined.

Several tests have been performed where the coupled model is compared to a 3D model. A good agreement between the models has been observed. The smoke distribution, but also the density, velocity and temperature distributions in the 3D model are well approximated with the coupled model.

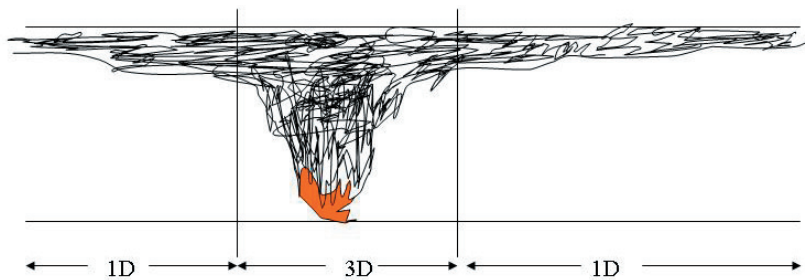


Figure 6  
The 3D and 1D regions

### User Interface

As there are normally limited capabilities inside a CAVE environment to input text and numbers, a new PDA-based graphical user interface (GUI) has been de-

veloped. This GUI allows the user to specify the mission he/she wants to examine, change simulation parameters and restart a simulation. The major advantage of this solution is that this navigation tool can also be used outside the CAVE with the PC-based VR environment without any changes to the simulator, because it is integrated into the network communication layer inside the simulator.

Navigation in space is supported by a space mouse device, by the navigations tools normally used in the CAVE environment or by the PDA. Navigation in time is possible by a simple “VCR-like” graphical user interface.

Within this user interface the user can create and define new missions, edit existing ones and start new calculations. The visualization system shows these new results as soon as they are available on the database server.

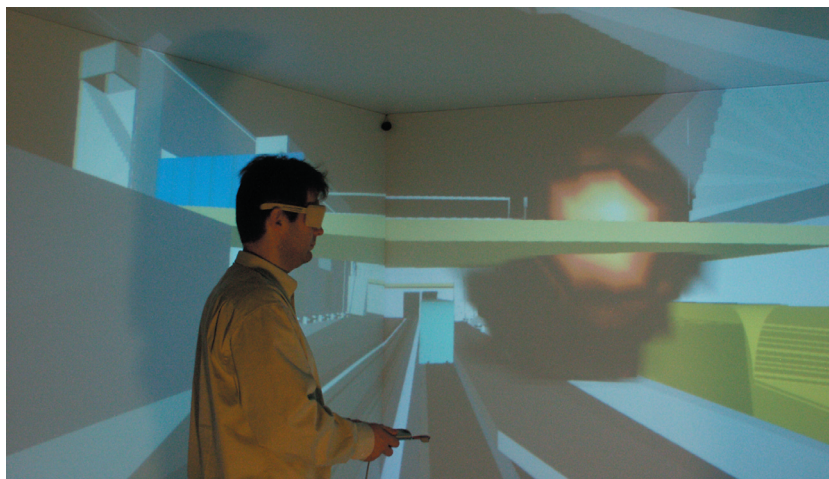
### Examples

For demonstration purposes some popular fire incidents have been calculated with the simulator. These datasets also serve as a base for the verification of the whole system.

The calculated dataset consists of different ventilation scenarios for the Mt. Blanc tunnel in France and the Gleinalm tunnel in Austria. Both tunnels were examined with their former ventilation system and also with the improved ones after the reopening. Examples of fire simulations are given in Figure 3 and Figure 4.

Also a typical subway station in Dortmund has been analyzed. In Figure 7 a fire inside the station on a subway train is visualized in the CAVE at PDC. Together with the calculation of smoke spread this kind of simulation is important for the firefighters to plan their missions inside these stations and to verify that their strategies are efficient.

Figure 7  
Fire in a Dortmund subway station  
simulated in the CAVE



## Conclusions

A simulator was presented which allows firemen to perform virtual training exercises with a PC, a head mounted display or in a CAVE environment. The simulator also allows assessing the fire safety of existing tunnels and can be used as a tool for designing new tunnels.

## References

1. D'Humieres, D., Ginzburg, I., Krafczyk, M., Lallemand, P., Luo, L.-S., Multiple-relaxation-time lattice Boltzmann models in three dimensions, *Phil. Trans. R. Soc. Lond. A* 360, pp. 437 – 452 (2002).
2. Yu, D., Mei, R., Luo, L.-S., Shyy, W., Viscous Flow Computations with the Method of Lattice Boltzmann Equation, *Prog. Aero. Sc.* 39, pp. 329 - 367 (2003).
3. COVISE, Vircinity GmbH, Nobelstraße 15, 70569 Stuttgart Germany, <http://www.vircinity.com>
4. Guo Z., Shi B., Zheng C., A coupled lattice BGK model for the Boussinesq equations, *Int. J. Numer. Meth. Fluids* 2002, 39:325-342
5. Luo, L.-S., The Lattice Gas and Lattice Boltzmann Methods: Past, Present, and Future, *Proceedings Int. Conf. Appl. Comp. Fluid Dyn.*, Beijing, China, October 17 – 20, 2000.



# The NeuroGenerator

## Functional Brain Image Database

Gert Svensson<sup>1</sup>, Lars Forsberg<sup>1,2</sup>, Per Roland<sup>2</sup>

<sup>1</sup>Center for Parallel Computers (PDC), Royal Institute of Technology (KTH), Stockholm

<sup>2</sup>Division of Human Brain Research, Department of Neuroscience, Karolinska Institutet, Stockholm

The European Commission funded project NeuroGenerator [1, 2] developed a database containing results from functional brain experiments as well as resulting statistically processed activation images. The processing is made within the system in a homogenous way, which makes it easier to compare and even combine result from different experiments and laboratories.

### Introduction

Imaging of the functions of the human brain is one of the most rapidly growing fields in neuroscience. The main objective is to map the location of cerebral functions. Two techniques that measure brain activities indirectly are Positron Emission Tomography (PET) and functional Magnetic Resonance Imaging (fMRI). PET measures the changes in blood flow and is based on measurements of the decay of a radioisotope injected in the human body. fMRI measures the oxygenation of blood indirectly by measuring the spin of protons in a strong magnetic field. The activity in the brain is interpreted from these measurements.

In a functional experiment the subject will repeatedly perform a specific task and/or be given different stimuli. The measured signals are extremely weak compared with the noise signal. To be able to obtain significant results statistical analysis is used often combined with manual tuning of different parameters. Many software packages [3, 4] exist for this kind of analysis.

Today different laboratories use different software packages and procedures for analysis making it hard to compare the results. The idea behind the NeuroGenerator database is to collect meta data such as the experiment protocol and raw measured data (data directly from the scanner), which will automatically be statistically analyzed in the system. Other databases in the field contain only the results [5, 6] or raw data and results but analyzed by the original laboratory using different procedures [7].

In the Neurogenerator database we also have cytoarchitectural data obtained by careful, partly manual, analysis of post mortem human brains [8].

Queries to the database can be submitted by a combined query and visualization tool called NeuroViz, which can combine meta data queries with 3D visual queries.

## System architecture

Figure 1  
NeuroGenerator system architecture

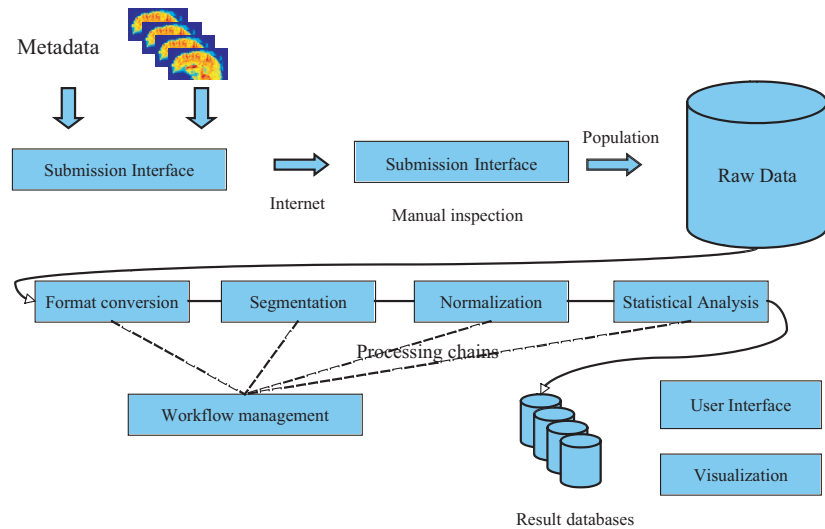


Figure 1 describes the overall architecture of the system. Experimental data from laboratories world wide can be submitted by a special submission interface. The experimental conditions have to be described in some detail together with the raw data images and sent over Internet to PDC where data is unpacked and quality assured, partly manually. If the experiment is approved the data is entered into the database. The raw data is stored in the tape robot at PDC and is after that treated in several steps in a processing chain. The first step in the chain is to transfer the images from the scanner to a common image format. The skull bone has to be removed by an image processing step called segmentation or de-boning. To be able to compare activations from different brains which have different sizes and shapes all the images are translated into a standard space by using a standard brain in a procedure called normalization.

The following statistical analysis uses in principle the general linear model (a general form of least square fitting) which gives areas of activation.

The processing of typical fMRI experiment takes approximately one or two days on a single node in Lucidor at PDC. However most of the steps in the analysis operate on single images and can be run in parallel.

The NeuroGenerator project is using the PostgreSQL database management system. Experiments are stored in a specific structure. This structure is comprehensive,

since it must give enough information both for the statistical analysis of the actual experiment and the meta-analysis across experiments. The experiment has a hierarchical structure. It is divided into conditions, subjects and interpretations.

### Experiment structure

A condition describes what is happening during the experiment, for instance a somatosensory discrimination condition. Each condition is given a name and a duration time, and is described in terms of events. A somatosensory discrimination condition is typically described with at least two somatosensory events and a response event, where the subject has to discriminate between e.g. the size of two objects and then respond which one was bigger. Each event is described with keywords and has a start time and a duration time within the condition. See Figure 2. The keywords also have a hierarchical structure. Each keyword, such as 'stimulus/somatosensory' can be divided into several sub-keywords. For instance, somatosensory is divided into skin, muscle and joints, and visceral. Skin in turn is divided into mechanoreceptive, chemical, electrical, and thermal. See Figure 3. A common condition is the rest condition, where the subject is just resting.

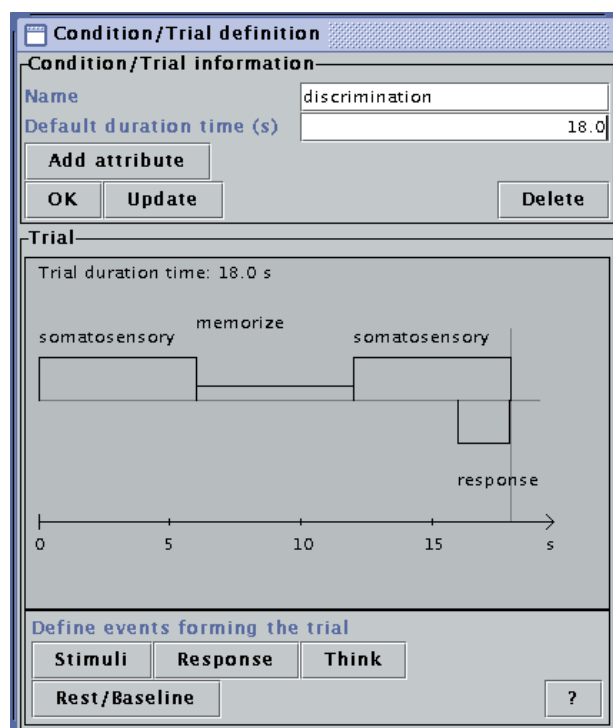


Figure 2  
The condition window in the submission interface displaying the time relation in a somatosensory experiment

A subject describes a human subject of the experiment. It is common that a subject is scanned several times. Each such time is called a session and gives a huge four dimensional file containing both spatial and temporal data of the subject's brain. All the sessions are also stored in the experiment structure, together with onset times for the different conditions. A subject is also described in terms of gender, handedness and age.

Another section describes the interpretation of the experiment. It holds a description how to generate the statistical images by subtracting one condition from another, for instance discrimination vs. rest. Such a mathematical expression is called a contrast.

The corresponding statistical image will in this case show what regions in the brain that are significantly more activated by the discrimination task compared to the rest state. We have developed special user defined functions in the database which enables us to query on the actual information in the images. This makes it possible to quickly find all contrasts having an activation in a certain brain region.

Figure 3  
A somatosensory stimuli described by a set of keywords

**Event definition**

**Event information**

Name: somatosensory

Start time (s): 0.0

Duration time (s): 6.0

Type: Stimulus

Buttons: OK, Update, Add attribute, Delete

**Keyword information**

Select keyword from the menu button below, then select additional keywords.

stimulus/somatosensory/skin/mechanoreceptive  Suggest own keywords

**bilateral/unilateral**

unilateral right ▼

**right topography**

oculomotor

head

neck

hand

?

## Submission procedure

Previous database projects in the field of human brain mapping have either tables describing the activations in a specific coordinate system, or statistical 3D images with a typical size of about 1 MB per image. A common experiment could, in the latter case, have a size of about 5 MB, corresponding to 5 statistical images.

The data submitted in the NeuroGenerator project is much larger in size since the actual native scanner data is submitted. A typical experiment is about 1 GB. The data is submitted with a Java application called the submission interface. Users can choose to submit either through the Internet with a proprietary protocol or send the data on CD:s or DVD:s. The submission interface has an automatic quality control, which checks for obvious errors such as missing information. The experiment is populated into the database after a manual quality procedure.

## Processing chains

The NeuroGenerator project receives both PET and fMRI experiments. The analysis is done in several steps, connected in a so called processing chain. The processing chain for fMRI is slightly more complicated than the processing chain for PET, but they both result in statistical 3D images called statistical parametric maps. The database stores these as Z-images, meaning the noise has a  $N(0,1)$  distribution. The null hypotheses is that there is no activation, and it is rejected whenever a value can be shown not to be  $N(0,1)$  distributed with a certain significance.

Since a statistical image contains many voxels and thus many measurements, the chance of getting one or more false positive voxels increase with the number of resolution elements (i.e. the number of independent voxels). This is referred to as the multiple comparison problem, which can be solved by using the gaussian random field maximum-height theory which takes into account the number of resolution elements [9]. An alternative method, also using gaussian random field theory, is based on the spatial extent of clusters of connected voxels after thresholding at some value  $z$  [10]. Here, the null hypotheses is applied on each cluster rather than the whole image. Rejecting it means that the cluster is significant. Clusters with a large spatial extent are more significant. Hence, it is possible to find significant clusters with a low  $z$ -threshold, given that the size of the clusters is large.

The final result is significant clusters for each contrast. These are populated into the database as binary 3D images, showing where in the brain we have significant clusters of connected voxels.

## Query and visualization tool

The image functions in the database can use the final result to find clusters that overlap certain brain regions. To facilitate this, we developed the visualization and

query tool NGViz which allows us to perform meta analysis across experiments. NGViz uses OpenGL for 3D volume rendering of the brain, which helps localizing both activations and anatomical structures such as gyri and sulci. It also supports 2D visualization, showing the brain in its horizontal, coronal and sagittal view.

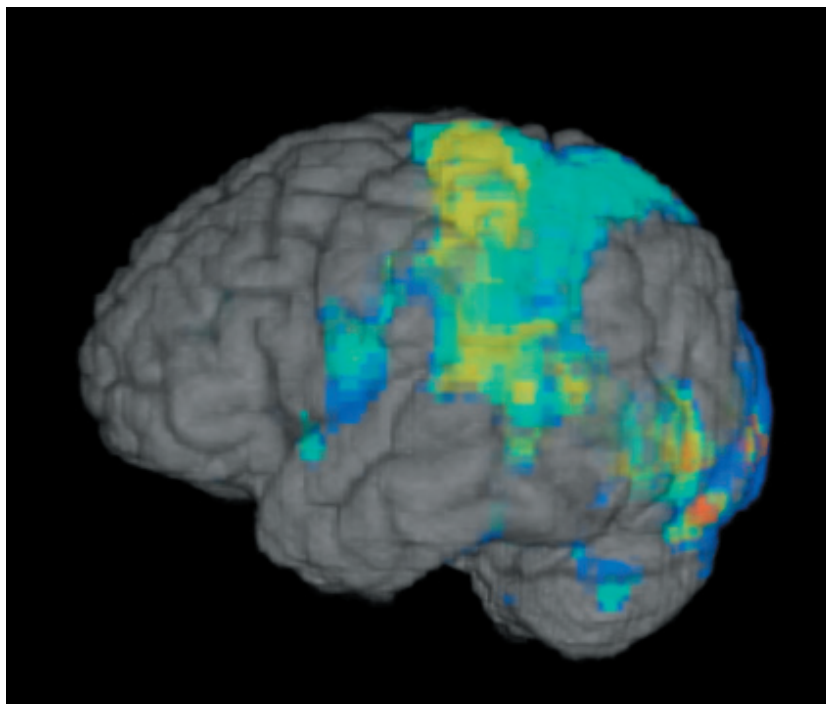
The query system is built upon four features:

1. Relating a selection of a table to other tables, allowing the user to browse through the database content.
2. Search within a specific table.
3. Search within a previous result.
4. Boolean operations between query results.

Using them together with the visualizer, the user can visualize the outcome from advanced queries such as:

1. Find all statistical brain images activating both cytoarchitectural areas 44, 45 (Broca's area) and cytoarchitectural area 17 (primary visual cortex, V1). See Figure 4 for a population map of the result.
2. Find all statistical brain images involving experimental conditions having somatosensory tasks. The control conditions should not have the same kind of task. See Figure 5 for a population map of the result.

Figure 4  
A population map of all images activating areas 44, 45 and 17.



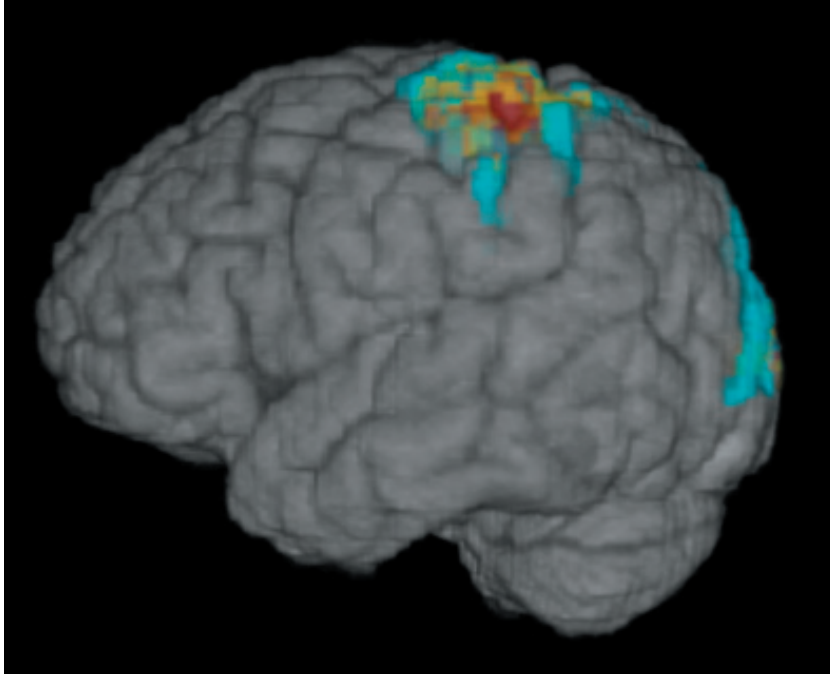


Figure 5  
A population map of all images having somatosensory tasks.

The population maps from these queries describe for each voxel the number of statistical results having a representation in that voxel. From the results, it is possible to ask further questions and get references to papers or read the method description provided by the database.

These queries show that it is possible to find relationships between certain tasks or cytoarchitectural areas and activations in the NeuroGenerator database by using the NGViz application. Since NGViz is provided as Open Source, it is possible to install it on almost any Unix operating system such as Linux, Mac OS X, FreeBSD, or Solaris.

### Meta analysis

A single study reveals just a few functions for the regions rejected by the null hypotheses. In reality, these regions are probably contributing to many more functions, together with other regions in a larger network. One study is thus not enough to draw any general conclusions about a particular cortical region in the cerebral cortex.

One of the primary functions of the NeuroGenerator database is to perform meta analysis across experiments. It helps studying brain implementation of vision, sen-

sory and motor systems, speech production, speech comprehension, memory and cognitive functions such as attention in normal subjects. With the NeuroGenerator database, it is thus possible to find common denominators for brain regions across experiments. This is possible since the statistical results are produced with the same analysis tools and processed in a homogenous way.

Two recent studies made from the NeuroGenerator database [11, 12] show that it is possible to find more information about a certain brain region by combining several experiments in a meta-analysis. This may give us new hypotheses about the brain's functionality, which can then be tested in a new PET or fMRI experiment.

This work was supported by the Foundation for Strategic Research in the BINS project and the European Commission in the Quality of Life program through the NeuroGenerator and Neurodisseminator projects.

## References

1. Roland, P; Svensson, G; Lindeberg, T; Risch, T; Baumann, P; Dehmel, A; Fredriksson, J; Halldorsson, H; Forsberg, L; Young, J; Zilles, K. A database generator for human brain imaging. *TRENDS in Neurosciences* 24(10), 562-564, 2001.
2. NeuroGenerator. Neurogenerator, Sep. 2004. <http://www.neurogenerator.org/>.
3. Wellcome Department of Imaging Neuroscience. SPM, Sep. 2004. <http://www.fil.ion.ucl.ac.uk/spm/>.
4. FMRIB. FSL, Sep. 2004. <http://www.fmrib.ox.ac.uk/fsl/>.
5. Fox, P; Lancaster, J. Mapping context and content: the BrainMap model. *Nature Reviews Neuroscience* 3, 319-321, 2002.
6. BrainMap. Brainmap, Sep. 2004. <http://ric.uthscsa.edu/projects/brainmap.html>.
7. fMRIDC. The fMRI Data Center – fMRIDC home page, Sep. 2004. <http://www.fmridc.org/>.
8. K. Zilles and N. Palomero-Gallagher. Cyto-, myelo-, and receptor architectonics of the human parietal cortex. *Neuroimage*, 14:S8–S20, 2001.
9. Worsley, K.J., Marrett, S., Neelin, P., Vandal, A.C., Friston, K.J., and Evans, A.C. (1996). A unified statistical approach for determining significant signals in images of cerebral activation. *Human Brain Mapping*, 4, 74-90.
10. Friston, K.J., Worsley, K.J., Frackowiak, R.S.J., Mazziotta, J.C., and Evans, A.C. (1994). Assessing the significance of focal activations using their spatial extent. *Human Brain Mapping*, 1, 214-220.
11. Young J., Forsberg L., Roland P. Task activating somatosensory and motor regions: a PET meta-analysis (2004). The 10th Annual Meeting of the Organization for Human Brain Mapping, Budapest 2004.

12. Forsberg L., Young J., Roland P. Somatosensory/motor interactions identified by PCA (2004). The 10th Annual Meeting of the Organization for Human Brain Mapping, Budapest 2004.



# Appendix I

## Hardware & Software Specifications

Current facilities (December 2003)

### Computing resources

#### Lucidor

A 90 node cluster equipped with dual 900 MHz Itanium2 (McKinley) processors. 1.5 MB L3 cache, 256 kB L2 cache and 16+16 kB L1 cache per processor. 6 GB RAM memory per node and 21 GB SCSI scratch disk. Nodes are interconnected with Myrinet 2000 rev. D providing 2×248 MB/s, 6.3 μs application level latency.

#### Nighthawk

Eight IBM Power3 222 MHz 8-way shared memory nodes, with each processor having 4 MB L2 cache and 32+64 kB L1 cache. Seven of the nodes have 4 GB RAM memory and one has 16 GB RAM. The nodes are interconnected with a 500 MB/s, 1 μs latency IBM SP Colony switch shared with the Kallsup computational resource.

#### Kallsup

Three IBM Power3 375 MHz 16-way shared memory nodes. One of the nodes is equally shared between the Kallsup consortium and VR. The cache properties are the same as for the Nighthawk system. Each node has 16 GB RAM memory.

#### LinuxLab/Roxette

16 IBM x340 servers equipped with Intel PIII 866 MHz processors, 256 kB L2 cache and 16+16kB L1 cache with 256 MB RAM memory per node and 100 Mbps Ethernet interconnect. 6 of the nodes were equipped with gigabit Ethernet cards at an early stage of gigabit Ethernet availability for technology testing and parallel filesystem evaluation. The system was donated by IBM in sponsoring PDC as one out of six European Linux Laboratories.

#### SBC

The Stockholm Bioinformatics Center resources at PDC at the end of 2003 consisted of an inhomogeneous cluster of 202 IA-32 nodes, and a few servers including a database server and three storage servers with a total of approximately 1.3 Tb of usable disk space. 100 Mb Ethernet is used for interconnect.

### **Boye**

A 12 CPU SGI Onyx2 system equipped with R10000 processors, 4 GB RAM, 3 Infinite Reality graphics pipes and 180 GB Fibre Channel disk.

### **SweGrid/Beppe**

A 100 node cluster equipped with a 2.8 GHz Intel P4 processor with 800 MHz front side bus, 2 GB RAM and an 80 GB 7200 rpm IDE hard disk on each node

### **Data storage resources**

The PDC infrastructure includes both disk systems for home directories and for temporary storage, and a tape library for backup and archival storage. A hierarchical storage management system (HSM) is used for file migration in the hierarchy, and a parallel file system is used for I/O for some of the compute resources, and being investigated for other resources.

#### **HSM and backup.**

The front-end server for HSM is an SGI Origin300 server with two R14000 CPUs @ 600 MHz, 1 GB RAM and approx. 300 GB disk. The front end server for backup is an IBM 7044-270 server with two PowerPC 630 CPUs, 1 GB of memory and 500 GB disk. The back-end system is an IBM 3494 IBM tape library Dataserver with four IBM 3590 Magstar tape drives. System software includes DMF from SGI and TSM from IBM. The capacity of the tape library has remained unchanged at 37 TB during the period which has posed a serious challenge for PDC to serve its users.

#### **GPFS**

A parallel file system serving the Nighthawk and Kallsup systems. The current configuration provides 780 GB of high-performance parallel disk storage.

### **Graphics and virtual reality resources**

#### **ImmersaDesk**

The PDC ImmersaDesk is driven by an SGI Octane computer equipped with 2 R10000 CPUs and a total of 1 Gbyte of memory and EMXI graphics. It is used for computation and visualization purposes.

#### **VR cube**

A fully immersive visualization environment forming a  $3 \times 3 \times 2.5\text{m}$  (W  $\times$  D  $\times$  H) room driven by Boye. The unique feature of this virtual reality system is the display of images on all surrounding surfaces, including the floor and the ceiling. Each of Boye's graphics pipes manages two of the six surfaces. The floor and ceiling

are currently configured for a resolution of  $1024 \times 1024$  pixels at a frequency of 96 Hz (i.e., 48 Hz per eye, due to stereo projection). The walls are configured for a resolution of  $1024 \times 852$  pixels to keep the pixels square and to keep the resolution constant along the edges.

For visualization the following software packages are available:

- Covise from VirCinity is a modular scientific visualization software with support for collaborative visualization and virtual reality displays.
- VMD is a molecular visualization program for displaying, animating, and analyzing large biomolecular systems using 3D graphics and scripting in Tcl or Python.
- The Visualization ToolKit (VTK) is an open source, freely available function library for 3D computer graphics, image processing, and visualization. Supported languages include C++, Tcl, Python and Java.
- OpenDX is an open source visualization system with a graphical user interface and a scripting language.
- AVS is a commercial modular visualization system with a graphical user interface.
- Saranav is a tool for immersive visualization of 3D models in a number of different formats.
- Navier is a PDC developed tool for immersive visualization of 3D models in a number of formats, with support for extending the visualization with interaction functions written in C++.
- Ygdrasil is a scripting language for developing interactive visualizations based on 3D models.
- Matlab is a numerical computation and visualization system.
- Maple is a symbolic algebra and geometry visualization system.

### Networking resources

PDC is connected directly to the KTH Network Operations Center, KTHNOC, via a dedicated 1 Gbps connection. KTHNOC is also managing the NOCs for Sunet and Nordunet. Internally, PDC has implemented a high-speed network infrastructure to support large-scale I/O and enable computational clusters of PDC systems. Two Extreme Black Diamond routers serve at the heart of the network with 1 Gbps Ethernet connections to other services. The Black Diamond routers support 10 Gbps ports.

Table 1  
Application software and libraries at PDC.

### Software

The application software available on the systems available for users of the VR resources is listed below. During this period the most noticeable changes are the installation of the Jaguar and NWChem packages in response to user needs. In connection with the installation of the NWChem package, developed at the Pacific Northwest National Lab in the US for scalable architectures, a workshop was held at PDC in 2000.

Biology	Chemistry/Physics	Engineering	Tools	Libraries
GeneHunter	CHARMM	ABAQUS	NAGware	METIS
GeneHunter-Plus	Dalton	Fluent	Foresys	PARMETIS
Allele Sharing	DL_POLY	StarCD	TotalView	Intel MKL
	GAMESS		Vampir	LAPACK
	Gaussian03		Dimemas	ScaLAPACK
	Gaussian98		PAPI	FFTW
	Jaguar		netCDF	ARPACK
	MacroModel		HDF4	WSSMP
	NWChem		HDF5	ESSL
	Molcas			PETSC
				PARPACK
				VML
				NAG





## Appendix II

### List of SNAC Projects at PDC

JANUARY 2000					
Principal Investigator	Affiliation	Project Title	IBM SP (h/month)	Fujitsu VX (h/month)	Period (months)
Asplund, Martin	UU	The nature of convection in stars		100	6
Boman, Magnus	LIU	Theoretical studies of conjugated polymers and molecular cellular automata		75	12
Davidson, Lars	CTH	Large Eddy simulation for computing the flow around vehicles	4000		6
Davidson, Lars	CTH	Large Eddy simulation of the flow around an airfoil using the IBM SP	8000		12
Elvingsson, Christer	UU	Dynamic processes in gel forming systems, especially associative polymers	600		6
Eriksson, Leif A	UU	Theoretical studies of processes in biological systems		450	12
Fuchs, Lazlo	LTH	Parallel large Eddy simulation of spray injection in gas turbines	3000		12
Häggkvist, Roland	UMU	Graph theory and statistical physics	4000		6
Juhlin, Christopher	UU	Modeling of seismic waves in 3-D heterogeneous media	500		6
Laaksonen, Aatto	SU	Hybrid QM MD approach to multiple reaction calculations in biological systems	1000		6
Laaksonen, Aatto	SU	Theoretical Photoimmunological studies of some biologically important chromophores using quantum mechanical O(N) simulations methods	1000		6
Linse, Per	LU	Statistics-mechanical modeling of polyelectrolyte-colloid systems	3000		6
Mattson, Thomas	KTH	Computational materials physics. From ab-initio calculations to materials properties	4000		12
Ojamäe, Lars	SU	Quantum-Chemical calculations and MD simulations of protonated water clusters, liquids and ice		475	12

Principal Investigator	Affiliation	Project Title	IBM SP (h/month)	Fujitsu VX (h/month)	Period (months)
Pettersson, Lars	SU	Metal oxide chemistry	2000		6
Rizzi, Arthur	KTH	Parallel computing for aircraft design	3000	200	12
Schimmelpfennig, Bernd	KTH	Magnetic molecules and spin labels	2000		6
Snis, Anders	CTH	Reactivity of metal and oxide clusters absorbed on a host substrate	1500		12
Stenholm, Stig	KTH	Laser physics and quantum optics		100	12
Thomas, John O.	UU	Computer-controlled development of optical polymer materials	2000		6
Thomas, John O.	UU	MD simulations of ion mobility in polymer surfaces and polymerorganic interfaces	3000		6
Ågren, Hans	KTH	Non-linear properties of molecules and extended systems	2000		6
Ågren, Hans	KTH	Wave packet dynamics in x-ray Raman scattering	1000		12
Öberg, Sven	LTU	First principle calculations of defect related properties in semiconductors	2000		6

JULY 2000						
Principal Investigator	Affiliation	Project Title	IBM SP (h/month)	IBM SP NH (h/month)	Fujitsu VX (h/month)	Period (months)
Asplund, Martin	KVA	The nature of convection in stars			150	12
Brinck, Tore	KTH	Quantum chemical studies of enzyme catalysis	2000			12
Davidson, Lars	CTH	Large Eddy simulation for computing the flow around vehicles	4000	200		12
Dorch, Bertil	KVA	Solar Magnet Fields and Dynamo Action			150	6
Dzugotov, Mikhail	KTH	Computer simulations study of phase transformation in icosahedrally coordinated metallic alloys		600		12

Principal Investigator	Affiliation	Project Title	IBM SP (h/month)	IBM SP NH (h/month)	Fujitsu VX (h/month)	Period (months)
Edholm, Olle	KTH	Computer simulations of lipid bilayers & parallel molecular dynamics software development		500		12
Elander, Nils	SU	Numerical studies of state-selective primary reactions and microwave-induced chemical reactions	2500		50	12
Fransson, Torsten	KTH	Forced response analysis and high cycle fatigue prediction of bladed-disk assemblies	5000	150	100	12
Hallberg, Anders	UU	Design and synthesis of protease inhibitors and turn peptidomimetics	700			12
Häggkvist, Roland	UMU	Graph theory and statistical physics		500		12
Johansson, Arne	KTH	Research on Turbulence and Transition	8000	300		6
Johansson, Patrik	CTH	Raman spectra and the disordered structure of inorganic glasses	2000			12
Juhlin, Christopher	UU	Modeling of seismic waves in 3-D heterogeneous media	500			12
Karlsson, Hans	UU	Simulations of femtosecond spectroscopy of triatomic molecules. Effects of non-adiabatic couplings	1000			12
Kowalewski, Josef	SU	Nuclear spin relaxation studies with applications to chemical problems	4000	200		12
Laaksonen, Aatto	SU	Quantum Molecular dynamics simulations methods	4000			12
Larsson, Karin	UU	Investigation of surface- and gas phase-reactions during film growth			100	6
Linse, Per	LU	Statistical-mechanical modeling of polyelectrolyte-colloid systems	2500			12
Mirbt, Susanne	UU	Magneto-electronics, Laser degradation, and spin-polarized STM		1500		12
Odelius, Michael	UU	Ab initio Molecular dynamics simulations of H-bonded systems and core-level x-ray spectra thereof	5000			6
Ottoson, Henrik	UU	A computational approach to questions in mechanistic organic chemistry: structure, stability, and reactivity	1000			6

Principal Investigator	Affiliation	Project Title	IBM SP (h/month)	IBM SP NH (h/month)	Fujitsu VX (h/month)	Period (months)
Persson, Mats	CTH	Electronic structure calculations for the physics of materials, surfaces and interfaces	5250			12
Pettersson, Lars	SU	Interfacial chemistry	3500			6
Rizzi, Art	KTH	Parallel computing for aircraft design	1000	200	100	12
Rosengren, Anders	KTH	Quantum XYZ spin-1/2 ladder with random rungs	4000			12
Ryde, Ulf	LU	Theoretical studies of the structure and function of metal proteins	6000			12
Salomonson, Sten	CTH	Two-photon QED corrections in highly-charged ions	3000	200		6
Sarman, Sten	GU	Molecular dynamics simulation of liquid crystals and alkanes	2500			12
Schimmelpfennig, Bernd	KTH	Magnetic molecules and spin labels	2500	200		12
Stafström, Sven	LIU	Computational studies of novel carbon based materials	1000			12
Svensson, Mats	KTH	Computational assisted design of new catalysts	1500		100	12
Szabó, Kálmán	SU	Computational studies on electronic and steric interactions	700			12
Wallin, Mats	KTH	Monte Carlo simulation of vortex dynamics in high temperature superconductors	4000			12
Widmalm, Göran	SU	Carbohydrate dynamics	5000			12
Öberg, Sven	LTU	First-principles calculations of defect related properties in semiconductors		1000		12

JANUARY 2001						
Principal Investigator	Affiliation	Project Title	IBM SP (h/month)	IBM SP NH (h/month)	Fujitsu VX (h/month)	Period (months)
Davidson, Lars	CTH	Large Eddy simulation of the flow around an airfoil using the IBM SP	4000			6

Principal Investigator	Affiliation	Project Title	IBM SP (h/month)	IBM SP NH (h/month)	Fujitsu VX (h/month)	Period (months)
Dorch, Bertil	KVA	Solar magnetic fields and dynamo action			200	6
Ehrenberg, Måns	UU	Stochastic simulations of genetic and metabolic networks	1000			12
Eriksson, Leif A	UU	Theoretical studies of biophysical systems			500	12
Gedde, Ulf W	KTH	Molecular dynamics simulation of diffusion of large molecules in amorphous polymer matrices	2000			12
Gedde, Ulf	KTH	Transport properties of hydrogen bonded polymers as revealed by molecular dynamics simulations	3000			6
Grimvall, Göran	KTH	Computational materials physics. From ab-initio calculations to materials science	3000			6
Henningsson, Dan	KTH	Research on turbulence and transition	9000			12
Kloo, Lars	KTH	The biological chemistry of Non-sexy cations	300			12
Larsson, Karin	UU	Investigations of surface- and gas phase- reactions during film growth			250	12
Mattson, Ann	KTH	Density functional theory for systems with electronic edges	2000			12
Ottoson, Henrik	UU	A computational study of mechanistic problems in organic chemistry	500			12
Pettersson, Lars G. M.	SU	Interfacial chemistry	4500			12
Salomonsson, Sten	CTH	Two-photon QED corrections in highly-charged ions	5000			12
Schimmelpfennig, Bernd	KTH	Magnetic molecules and spin labels	2500	200		12
Siegbahn, Per	SU	Mechanics for redox enzymes	2000			12
Ågren, Hans	KTH	Non-linear properties of molecules and extended systems	3000	100		12

JULY 2001							
Principal Investigator	Affiliation	Project Title	IBM SP (h/month)	IBM SP NH (h/month)	Fujitsu VX (h/month)	Mass Storage	Period (months)
Abrikosov, Igor	UU	First-principles calculations of fundamental properties of steels.	3000				12
Björling, Mikael	HIG	Statistical mechanics for Surfactants, Amphiphilic polymers, and Simple Liquids	50				12
Bolton, Kim	CTH	Computational studies of cluster reactions		200			6
Brinck, Tore	KTH	Quantum Chemical Studies of Enzyme Catalysis (Continued Project)	2000				12
Chattopadhyaya, Jyoti	UU	Conformational analysis of antisense oligonucleotide/RNA duplexes as substrates for RNase H	2000				12
Davidson, Lars	CTH	Large Eddy Simulation of the Flow around an Airfoil using the IBM SP	4000	500			12
Dorch, Bertil	SU	Solar Magnetic Fields and Dynamo Action			300	X	12
Edholm, Olle	KTH	Computational Studies of Lipid Membranes & Parallel Molecular Dynamics Software Development	3000	250		X	12
Elander, Nils	SU	Computer modeling of chemical reaction mechanisms: Resonances building blocks in studies of primary chemical reactions and processes in Microwave-Enhanced Chemistry.	1000	400			12
Engquist, Björn	KTH	Particular Flow Simulator - A System for Direct Simulation and Derivation of Bulk Models		300			12
Fransson, Torsten	KTH	Numerical Investigation of Transition, Flutter and Forced Response in Axial Turbomachines	5000	150		X	12
Gogoll, Adolf	UU	Development of peptide mimetics capable of externally triggered conformational changes	700				12
Grimvall, Göran	KTH	Computational materials physics. From ab-initio calculations to materials properties.	3000				12

Principal Investigator	Affiliation	Project Title	IBM SP (h/month)	IBM SP NH (h/month)	Fujitsu VX (h/month)	Mass Storage	Period (months)
Haefner, Fredrik	SU	The Mechanism of Catechol Cleavage Catalyzed by the Extra and Intra Diol Dioxygenases. A Density Functional Study.	1400		400		12
Häggkvist, Roland	UMU	Graph Theory and Statistical Physics		400			12
Johansson, Patrik	CTH	Molecular Species at Nano-Particle Surfaces: Adsorption and Vibrational Spectra	3000	300			12
Karlsson, Hans	UU	Quantum dynamics of triatomic molecules.	200	100			12
Kowalewski, Jozef	SU	Nuclear spin relaxation studies with applications to chemical problems	3000	200			12
Laaksonen, Aatto	SU	Expanded ensemble molecular dynamics simulations of ubiquinone in a membrane	4000	300			6
Lyubartsev, Alexander	SU	Quantum molecular dynamics simulation methods	3000				12
Mirbt, Susanne	UU	Calculation of magnetic-, defect-, and surface- properties		1500			12
Persson, Mats	CTH	Electronic Structure Calculations for the Physics of Materials, Surfaces, and Interfaces	4500	500		X	12
Piskunov, Nikolai	UU	Numerical Simulations of the Convective Envelopes of Red Supergiants		200			12
Rizzi, Arthur	KTH	CFD simulations of vehicle aerodynamics	200		100	X	12
Ryde, Ulf	LU	Theoretical studies of the structure and function of metal proteins	6000				12
Sarman, Sten	GU	Transport properties of liquid crystals and alkanes	3000				12
Sjöström, Sören	LIU	Fatigue life of thermal barrier coatings	600				12
Stafström, Sven	LIU	Transport properties of conjugated carbon based systems		300			12
Svensson, Mats	KTH	Computational Assisted Design of New Catalysts	1500		300		12

Principal Investigator	Affiliation	Project Title	IBM SP (h/month)	IBM SP NH (h/month)	Fujitsu VX (h/month)	Mass Storage	Period (months)
Szabó, Kálmán	SU	Computational Studies on Electronic and Steric Interactions Governing the Reactivity and Selectivity in Transition Metal-Catalyzed Transformations	900				12
Söderlind, Paul	HHS	A Monte Carlo study of measures of misspecification of asset pricing models	3000				6
Thomas, John O.	UU	QM- and MD-studies of ions in polymers	2000			X	12
Wallin, Mats	KTH	Monte Carlo simulation of condensed matter systems	4000				12
Widmalm, Göran	SU	Carbohydrate Dynamics	5000				12
Öberg, Sven	LUTH	First-principles modeling solids and molecules	4000	500			12

JANUARY 2002							
Principal Investigator	Affiliation	Project Title	IBM SP (h/month)	IBM SP NH (h/month)	Fujitsu VX (h/month)	Mass Storage	Period (months)
Amberg, Gustav	KTH	Numerical simulation of weld pools	3000				12
Bolton, Kim	CTH	Computational studies of cluster reactions	200				12
Brandt, Peter	KTH	Grundläggande principer för asymmetrisk induktion inom katalys och design av nya katalytiska system.	500				6
Henningson, Dan S.	KTH	Proposal for Research on Turbulence, Transition and Control	8000				12
Larsson, Karin	UU	Investigations of surface and gas phase reactions during film growth	500		500		12
Lindfelt, Ulf	LIU	Theoretical Investigations of the Electronic Structure of Dislocations, Stacking Faults and Polytype Inclusions.	5000				6
Luo, Yi	KTH	Theoretical studies of molecular photonics, biophotonics and electronics	1000				12

Principal Investigator	Affiliation	Project Title	IBM SP (h/month)	IBM SP NH (h/month)	Fujitsu VX (h/month)	Mass Storage	Period (months)
Pettersson, Lars G.M.	SU	Hydrogen-bonded and biomimetic systems	5000				12
Rizzi, Arthur	KTH	CFD simulations of vehicle aerodynamics	1000		600	X	12
Salomonson, Sten	CTH	Two-Photon QED Corrections in Highly Charged Ions	2500				12
Schimmelpfennig, Bernd	KTH	Spin-Dependent Magnetic Properties of Molecules	4500				12
Siegbahn, Per E.M.	SU	Mechanisms for redox enzymes	2000				12
Wahlgren, Ulf	SU	Quantum Chemical Studies of Actinides Complexes in Solutions	500				12
Wallenius, Jan	UU	Radiation damage in Fe-Cr alloys: electronic structure calculations		500			12
Ågren, Hans	KTH	Optical and x-ray characterization of molecular materials	3000				12

JULY 2002							
Principal Investigator	Affiliation	Project Title	IBM SP (h/month)	IBM SP NH (h/month)	Fujitsu VX (h/month)	Mass Storage	Period (months)
Ahlberg, Per	GU	Studies of reactants and activated complexes in chiral lithium amide catalysed deprotonations. Design of novel catalysts.	2000				12
Brinck, Tore	KTH	Quantum Chemical Studies of Enzyme Catalysis	1500	300			12
Davidson, Lars	CTH	Large Eddy Simulation of the Flow around an Airfoil using the IBM SP	8000				12
Dorch, Bertil	SU	Solar Magnetic Fields and Dynamo Action			300	X	12
Edholm, Olle	KTH	Molecular dynamics simulations of biological model membranes and membrane proteins	3000	250			12

Principal Investigator	Affiliation	Project Title	IBM SP (h/month)	IBM SP NH (h/month)	Fujitsu VX (h/month)	Mass Storage	Period (months)
Elander, Nils	SU	Computational studies of resonances as building blocks in a description of primary chemical reactions	300	300			12
Fransson, Torsten	KTH	Numerical Investigation of Unsteady Flow, Transition, Flutter, Forced Response, Fluid-Structure Interaction and Radiation Phenomena in Axial Turbomachines	4000			X	12
Fuchs, Laszlo	LTH	Development of tools for the design of low emissions Gas Turbine burners	1000				12
Gogoll, Adolf	UU	Development of peptide mimetics capable of externally triggered conformational changes	1000				12
Grönbeck, Henrik	CTH	Structural, Dynamical and Chemical Properties of Supported Catalytic Particles	2000				12
Göthelid, Mats	KTH	Activity and Selectivity in Heterogeneous Catalysis	3000				6
Haeffner, Fredrik	SU	Catalysis of Hydrogen Peroxide Formation by the Beta-Amyloid Peptide-Cu(II) Complex. Implications for the Involvement of Oxidative stress in Alzheimer's Disease.	3000			X	12
Johansson, Patrik	CTH	Anion-Cryptand Complexes: Supramolecular Anions	3000	400			12
Lindfelt, Ulf	LIU	Theoretical Investigations of the Electronic Structure of Dislocations, Stacking Faults and Polytype Inclusions	3000				6
Lyubartsev, Alexander	SU	Multiple scale computer simulations	5000				12
Mirbt, Susanne	UU	Magneto-electronics, Laser Degradation, and STM-calculations		1500			12
Persson, Mats	CTH	Electron-structure calculations for the physics of materials, surfaces and interface	3500	1000		X	12
Rizzi, Arthur	KTH	CFD simulations of vehicle aerodynamics	600		600	X	12

Principal Investigator	Affiliation	Project Title	IBM SP (h/month)	IBM SP NH (h/month)	Fujitsu VX (h/month)	Mass Storage	Period (months)
Szabo, Kalman	SU	Computational Studies on Electronic and Steric Interactions Governing the Reactivity and Selectivity in Transition Metal-Catalyzed Transformations	900				12
Sörensen, Niels	LU	Investigation of strain localisation in polycrystalline materials subjected to idealized rolling conditions.	1400	400			12
Thomas, Josh	UU	Computer-aided battery and fuel cell materials	5000			X	12
Uvdal, Per	LU	Ab initio calculation of organo-metallic complexes as models for surface adsorbates	1000				12
Wallin, Mats	KTH	Monte Carlo simulation of condensed matter system	4000	1500			12
Widmalm, Göran	SU	Carbohydrate dynamics	8000				12
Öberg, Sven	LU	First-principles modeling of solids and molecules	8000				12

JANUARY 2003							
Principal Investigator	Affiliation	Project Title	IBM SP (h/month)	IBM SP NH (h/month)	Fujitsu VX (h/month)	Mass Storage	Period (months)
Amberg, Gustav	KTH	Simulation of Welding Pool	4000			X	6
Dzugotov, Mikhail	KTH	Molecular Dynamics Simulation of Condensed Matter	4000	500		X	12
Henningson, Dan	KTH	Proposal for research on turbulence, transition and control	10000				12
Johansson, Patrik	CTH	Quantum mechanical global optimization of lithium salts	1000				12
Johnson, Tobias	GU	Quantum Chemical Investigations on the Mechanisms for Hydrogen Peroxide Formation	1000				12

Principal Investigator	Affiliation	Project Title	IBM SP (h/month)	IBM SP NH (h/month)	Fujitsu VX (h/month)	Mass Storage	Period (months)
Larsson, Karin	UU	Effect of Chemical Composition and Nano-Sizes on Materials Properties	500				12
Luo, Yi	KTH	Theoretical studies of molecular photonics, biophotonics and electronics	1000				12
Moberg, Christina	KTH	Quantum chemical study of catalytic properties of organo-metallic complexes.	1500				12
Odelius, Michael	UU	Ab initio Molecular Dynamics and Density Functional Studies of Electronic Excitations	1200				6
Onipko, Alexander	LUTH	Modeling structure and phase behavior of functionalized, self-organized assemblies: Implications for molecular electronic devices and sensors	1000				12
Pettersson, Lars G.M.	SU	Interfacial chemistry	5000				12
Rizzi, Arthur	KTH	CFD simulations of vehicle aerodynamics	2000		1000	X	12
Siegbahn, Per	SU	Reaction mechanisms for metalloenzymes	1500				6
Sjögreen, Björn	KTH	High performance PDE solvers for combustion and astrophysics.	3000				12
Ögren, Hans	KTH	Computational Biochemistry and Biophysics	3000				12

JULY 2003							
Principal Investigator	Affiliation	Title	IBM SP (h/month)	IBM SP NH (h/month)	Mass Storage	Period (months)	
Abrikosov, Igor	UU	Electronic theory of materials properties: from fundamental understanding towards materials design	1500	2500		12	
Ahuja, Rajeev	UU	High Pressure Studies of Hydrogen and its Implications to Materials Science	3000			12	
Amberg, Gustav	KTH	Simulations of phase change and fluid flow in materials science		1500		12	

Principal Investigator	Affiliation	Title	IBM SP (h/month)	IBM SP NH (h/month)	Mass Storage	Period (months)
Brinck, Tore	KTH	Quantum Chemical Studies of Enzyme Catalysis	1500	200		12
Dorch, Bertil	SU	Solar Magnetic Fields and Dynamo Action	1000			12
Elander, Nils	SU	Mechanisms in chemical dynamics - The role of intermediate short-lived quantum states.	400	100		12
Fransson, Torsten	KTH	Numerical Investigation of Unsteady Flow, Flutter, Forced Response, Transition and Fluid-Structure Interaction in Axial Turbomachines	4000		X	6
Grönbeck, Henrik	GU	Fundamental Processes Governing Sintering of Metal Particles on Oxide Supports	2000			12
Helsing, Bo	CTH	Phonons and electron-phonon coupling at metal surfaces	100			12
Henelius, Patrik	KTH	Quantum Monte Carlo simulations of spin systems	1000			12
Häggkvist, Roland	UMU	Graph Theory and Statistical Physics	3000			12
Johansson, Patrik	CTH	Anion-Cryptand Complexes: Formation, Conformational Equilibrium, Dynamics, and Lithium Ion Affinities	1500			12
Korzhavyi, Pavel	KTH	Ab initio calculations of fundamental material properties of intermetallic compounds and transition metal-metalloid systems	5000			12
Laaksonen, Aatto	SU	Theoretical studies of a human DNA repair enzyme	5000	1500		12
Lansner, Anders	KTH	Implementation and benchmarking of a scalable brain-like computer architecture	100			6
Larhed, Mats	UU	Computational Studies of Stereo- and Regioselective Heck Transformations	1500			12
Lieberman, Michael	UU	Combustion research and numerical modeling for developing low-emission and high-efficient energy technologies	2500			12
Lidmar, Jack	KTH	Monte Carlo Simulations of Vortices in Superconductors	5000			12
Lidström, Per	LU	Micromechanical and overall investigations of engineering materials.	1000	200		12

Principal Investigator	Affiliation	Title	IBM SP (h/month)	IBM SP NH (h/month)	Mass Storage	Period (months)
Lund, Björn	UU	Modeling the effects of deglaciation on the crustal stress field in northern Scandinavia and implications for postglacial faulting.	2000	500	X	12
Lyubartsev, Alexander	SU	Multiple Scale Computer Simulations	5000			12
Mirbt, Susanne	UU	Spintronics, Defects in semiconductors, and spin-polarized STM.		500		12
Persson, Mats	CTH	Electron-structure calculations for the physics of materials, surfaces and interfaces	7500	1000	X	12
Siegbahn, Per	SU	Reaction mechanisms for metalloenzymes	1500			12
Szabo, Kalman	SU	Computational Studies on Electronic and Steric Interactions Governing the Reactivity and Selectivity in Transition Metal-Catalyzed Transformations	900			12
Thomas, Josh	UU	Modeling polymers for battery and fuel cell applications	2000			12
Vahtras, Olav	KTH	Density functional calculations of magnetic resonance parameters of radicals	2000			12
Widmalm, Göran	SU	Carbohydrate dynamics	5000			12
Öberg, Sven	LU	First-principles modeling solids and molecules	3000			12

JANUARY 2004							
Principal Investigator	Affiliation	Title	Itanium (h/month)	IBM SP (h/month)	IBM SP NH (h/month)	Mass Storage	Period (months)
Belonoshko, Anatoly	KTH	Computer experiment in condensed matter physics	1000				12
Björling, Mikael	HIG	Interaction potentials between simple fluorocarbons			100		6
Bondeson, Anders	CTH	Computational Electromagnetics and Magnetohydrodynamics	100		100		12
Dieckmann, Mark Eric	LIU	Investigations of the interaction between large amplitude electrostatic waves with plasma	1000				12

Principal Investigator	Affiliation	Title	Itanium (h/month)	IBM SP (h/month)	IBM SP NH (h/month)	Mass Storage	Period (months)
Eriksson, Leif	UU	Theoretical studies of biophysical systems	3000				12
Fransson, Torsten	KTH	Numerical Investigation of Unsteady Flow, Flutter, Forced Response, Transition and Fluid-Structure Interaction in Turbomachines	1000		500	X	12
Henningson, Dan	KTH	Research on Turbulence, Transition and Control	2000				12
Johansson, Borje	UU	A theoretical study of fullerenes on surfaces	2000				12
Lansner, Anders	KTH	A scalable design of a brain-like computer for real-time execution	2000				12
Larsson, Karin	UU	Effect of Chemical Composition and Nano-Sizes on Materials Properties	2000				12
Luo, Yi	KTH	Theoretical studies of molecular photonics, biophotonics and electronics			500		12
Långström, Bengt	UU	Rationalization and Optimization of the Properties of Good PET Tracers	500		100		6
Pettersson, Lars G.M.	SU	Chemistry in Condensed Phase	2000				12
Privalov, Timofei	KTH	Ab initio studies of properties-to-function relations of actinide selective organic ligands and organo-metallic complexes.	1000				12
Rizzi, Arthur	KTH	CFD simulations of vehicle aerodynamics	1000		500	X	12
Salek, Pawel	KTH	Development and application of linearly-scaling ab-initio program for molecular properties	1000				12
Wahlgren, Ulf	SU	Ab initio studies of properties, kinetics and chemistry of heavy elements particularly in optically excited states.	1000				12
Ågren, Hans	KTH	Quantum Modeling of Molecular Materials	5000		500		12
Öberg, Sven	LUTH	First-principles calculations of properties modelled in large atomic clusters or supercells.	2000				6



## Appendix III

### Publications and Presentations by PDC

#### Journal publications

- Fredrik Hedman and Aatto Laaksonen, “Parallel aspects of quantum molecular dynamics simulations of liquids”, *Computer Physics Communications*, vol. 128, pp. 284 – 294, 2000.
- S. Lennart Johnsson with Francine Berman, Andrew Chien, Keith Cooper, Jack Dongarra, Ian Foster, Dennis Gannon, Ken Kennedy, Carl Kesselman, John Mellor-Crummey, Dan Reed, Linda Torczon and Rich Wolski, “The GrADS Project: Software Support for High-Level Grid Application Development”, *Journal of High-Performance Computing Application*, Vol. 15, No. 4, pp. 327 – 344, 2001.
- S. Lennart Johnsson with Ken Kennedy, Bradley Broom, Keith Cooper, Jack Dongarra, Rob Fowler, Dennis Gannon, John Mellor-Crummey and Linda Torczon, “Telescoping Languages: A Survey for Automatic Generation of Scientific Problem-Solving Systems from Annotated Libraries”, *Journal of Parallel and Distributed Computing*, Vol. 61, No. 12, pp. 1802 – 1826, 2001.
- S. Lennart Johnsson with Y. Charlie Hu, Guohua Jin, Dimitris Kehagias and Nadia Shalaby, “HPFBench: A High Performance Fortran Benchmark Suite”, *ACM Transactions on Mathematical Software*, Vol. 26, No. 1, pp. 99 – 149, March, 2000.
- Gert Svensson and Lars Forsberg with Per Roland, Tony Lindeberg, Tore Risch, Peter Baumann, Andreas Dehmel, Jesper Fredriksson, Hjörleifur Halldórsson, Jeremy Young and Karl Zilles, “A database generator for human brain mapping”, *Trends in Neurosciences*, Vol. 24, Issue 10, pp. 562-564, 2001.
- Per Öster with Alik Ismail-Zadeh, Igor Tsepelev, Christopher Talbot, “Three-dimensional modelling of salt diapirism: A numerical approach and parallel algorithm” (in Russian). *Computational Seismology and Geodynamics*, Vol. 31, pp. 62 – 76, 2000.

#### Refereed conference papers and book chapters

- Ulf Andersson, Per Ekman and Per Öster, “Performance and performance counters on the Itanium 2 – A benchmarking case study”, in ParCo2003 proceedings, 2003.
- Ulf Andersson and Fredrik Hedman, “Performance of an IBM pwr4 node for the GEMS TD codes and Parallacs”, in Fagerholm, Juha and others (Eds.) Applied Parallel Computing, PARA 2002, pp. 467 – 475, (Lecture Notes in Computer Science, No. 2367), 2002.

- Johan Danielsson with Assar Westerlund, Heimdal and Windows 2000 Kerberos - how to get them to play together, USENIX Annual Technical Conference, 2001.
- Johan Danielsson with Assar Westerlund, Different database methods in Heimdal, Management and Administration of Distributed Environments Workshop, 2000.
- Sten-Olof Hellström, Kai-Mikael Jää-Aro and Aatto Laaksonen, "Perceptualisation of molecular dynamics data", Highlights in Molecular Dynamics, 2000.
- S. Lennart Johnsson, "CODELAB: A Developers' Tool for Efficient Code Generation and Optimization", ICCS 2003, June 2 – 4, 2003, Melbourne, Australia.
- S. Lennart Johnsson with Ken Kennedy, Mark Mazina, John Mellor-Crummey, Keith Cooper, Linda Torczon, Fran Berman, Andrew Chien, Holly Dail, Otto Sievert, Dave Angulo, Ian Foster, Dennis Gannon, Lennart Johnsson, Carl Kesselman, Ruth Aydt, Daniel Reed, Jack Dongarra, Sathish Vadhiyar, and Rich Wolski, "Toward a Framework for Preparing and Executing Adaptive Grid Programs", Proceedings of NSF Next Generation Systems Program Workshop (International Parallel and Distributed Processing Symposium 2002), Fort Lauderdale, FL, April 2002.
- S. Lennart Johnsson, "Automatic Performance Tuning in the UHFFT Library", The 2001 International Conference on Computational Science, ICCS 2001, Hilton San Francisco and Towers, San Francisco, USA, May 28 – 30, 2001.
- S. Lennart Johnsson, "An Adaptive Software Library for Fast Fourier Transforms", 2000 International Conference on Supercomputing, pp. 215 – 224, ACM Press, May 2000.
- S. Lennart Johnsson, "SimDB: A Problem Solving Environment for Molecular Dynamics Simulation and Analysis", First European Grid Forum Workshop, pp. 321 – 329, in "Proceedings of ISThmus 2000: Research and Development for the Information Society", ISBN 83-913639-0-2, April 2000.
- Olle Mulmo with co-authors, "Next-Generation EU DataGrid Data Management Services." In Computing in High Energy Physics (CHEP 2003), La Jolla, California, March 2003.
- Olle Mulmo with co-authors, "Managing Dynamic User Communities in a Grid of Autonomous Resources." In Computing in High Energy Physics (CHEP 2003), La Jolla, California, March 2003.
- N. Smeds, "OpenMP application tuning using hardware performance counters". OpenMP Shared Memory Parallel Programming: International Workshop on OpenMP Applications and Tools, WOMPAT 2003, Toronto, Canada, June 26-27. Springer LNCS, Vol. 2716, Springer Verlag, 2003.

- Nils Smeds with Russell K. Standish, Clinton Chee, “OpenMP in the Field: Anecdotes from Practice”. International Conference on Computational Science 2003. In Springer LNCS, Vol. 2660, pp. 637-647, 2003.
- Nils Smeds, “Performance Tuning Using Hardware Counter Data”, Shirley Moore, University of Tennessee; Supercomputing 2001, Denver, Colorado.

## Books

- S. Lennart Johnsson with B. Engquist, M. Hammill and F. Short, Editors, “Simulation and Visualization on the Grid”, Editors, *Lecture notes in Computational Science and Engineering*, Springer-Verlag, Vol. 13, 300 pages, 2000.

## Reports

- Per Alexius, “Parallelization of software for simulation and optimization of military and civil operations. Computational enhancement of STRATMAS – the strategic management system”, M.S.Thesis, TRITA-NA-E02128, 2002
- Sarah Amandusson, “Auditory display and the VTK sonification toolkit”, M.S. Thesis, TRITA-NA-E03144, 2003
- Ulf Andersson, “The Gems TD benchmark suite”, TRITA-PDC 2003:2, 2003; Available at [http://www.pdc.kth.se/info/research/trita/PDC\\_TRITA\\_2003\\_2.pdf](http://www.pdc.kth.se/info/research/trita/PDC_TRITA_2003_2.pdf).
- Ulf Andersson, “Case Study: Computational Electromagnetics - The FDTD Method”, HPC Summerschool material, 2003.
- Ulf Andersson and Björn Engquist, “Regularization of material interfaces for finite-difference methods for the Maxwell equations”, TechReport 2002-01, Stockholm, 2002; Available at <http://www.psci.kth.se/Activities/Reports/List.html>.
- Ulf Andersson, “Yee\_bench – A PDC benchmark code”, TRITA-PDC 2002:1, 2002; Available at [http://www.pdc.kth.se/info/research/trita/PDC\\_TRITA\\_2002\\_1.html](http://www.pdc.kth.se/info/research/trita/PDC_TRITA_2002_1.html).
- Per Ekman, ”Visualisering av isflöden i glaciärer i en immersiv miljö”, M.S.Thesis, TRITA-NA-E0071, 2000
- Christian Engström, “Keep it simple and you will finish what you start -- a case study of the NeuroGenerator database project”, M.S.Thesis, TRITA-NA-E03021, 2003
- Fredrik Hedman, “C++ by Examples”, HPC Summerschool material, 2001.
- Niklas Jakobsson, “CAD to Cave”, M.S.Thesis, 2000
- Kai-Mikael Jää-Aro with Tomas Weber, “Virtualfires Project Deliverables D4.1 & D4.2: Specification of methods of displaying CFD data Specification of immersive user interface”, 2002.

- Kai-Mikael Jää-Aro and Erik Engquist, “Visualization”, HPC Summerschool material, 2001.
- Kai-Mikael Jää-Aro, Björn Sjögreen, Gert Svensson with José Luis Ajuria, Christian Redl and Wilhelm Brandstätter, “Virtualfires D2.1+2.3 Project Deliverable: Report on available developer tools, Report on available system capabilities (hardware)”, 2001.
- Olle Mulmo with co-authors, “European DataGrid EU Deliverable 7.6: Security Design Report.”, March 2003.
- Horacio Palomino, “Visualization of 3D Numerical Simulations in Astrophysics using the VR-cube”, M.S. Thesis, TRITA-NA-E03111, 2003.
- Sergei I. Simdyankin & Mikhail Dzugutov: Case Study: Computational Physics – The Molecular Dynamics Method, TRITA-PDC Report 2003:1, 2003.
- Gert Svensson and Kai-Mikael Jää-Aro with Sascha Schneider, Michael Schmidt, Volker Luckas, Gunther Lenz, Thomas Reichl, “Virtualfires WP 2.5 Project Deliverable: Review of existing VR systems”, Adaptability to VIRTUALFIRES, 2002.
- Gert Svensson, Kai-Mikael Jää-Aro with Sascha Schneider, Michael Schmidt, Volker Luckas, Gunther Lenz, Thomas Reichl, Wilhelm Brandstätter, Christian Redl, Alain Bochon, René-Michel Faure, Klaus Schäfer, Rainer Koch, José Luis Ajuria and Christian Redl, “Virtualfires WP 2.6 Project Deliverable: Review of existing VR systems”, Adaptability to VIRTUALFIRES, 2002.
- Gert Svensson, Kai-Mikael Jää-Aro with Sascha Schneider, Michael Schmidt, Volker Luckas, Gunther Lenz, Thomas Reichl, Wilhelm Brandstätter, Christian Redl, Alain Bochon, René-Michel Faure, Klaus Schäfer, Rainer Koch, José Luis Ajuria and Christian Redl, “Virtualfires Project Deliverable 2.2+2.4: Selection of developer tools”, Specification of planned system capabilities (software), 2002.
- Per Öster, “Fortran 90 by Examples”, HPC Summerschool material, 2001.

### Conference Exhibits and Live Demonstrations

- S. Lennart Johnsson, Erik Engquist and Per Öster, GEMSViz: Computational Steering of Electromagnetic Field Calculation from a Virtual Environment”, *iGRID 2000*, Yokohama, July 17 - 21, 2000.

### Presentations

- S. Lennart Johnsson: “Characterization of Application Behavior on IPF-Based Servers”, HP Executive Forum, Grenoble, December 5, 2003.
- Per Öster: “Grid i praktiken”, Oracle Technology Days, Stockholm, December 4, 2003 and Göteborg, December 5, 2003.

- Thomas Sandholm: “SweGrid Accounting System”, 6th NorduGrid Workshop, Lund, November 28, 2003.
- Ulf Andersson, Per Ekman, Per Öster: “Performance and performance counters on the Itanium 2 – A benchmarking case study “, Gelato Annual Meeting, Stockholm, October 26, 2003.
- S. Lennart Johnsson: “Grid Computing”, Gelato Annual Meeting, Stockholm, October 26, 2003.
- S. Lennart Johnsson: “Grid Computing – Application Development”, Baylor College of Medicine, Houston, September 26, 2003.
- Michael Hammill, “MPI Collective Communication”, National Graduate School of Scientific Computing, Stockholm, August 26, 2003 (and August 28, 2000, August 28, 2001, August 27, 2002).
- Michael Hammill, “Introduction to MPI”, National Graduate School of Scientific Computing, Stockholm, August 25, 2003 (and August 24, 2000, August 26, 2002).
- Michael Hammill, “MPI Point-to-Point Communication”, National Graduate School of Scientific Computing, Stockholm, August 25, 2003 (and August 25, 2000, August 28, 2001, August 26, 2002).
- S. Lennart Johnsson: “Grid Computing: Application Development”, National Graduate School of Scientific Computing, Stockholm, August 19, 2003.
- Michael Hammill, “Welcome to the PDC Summer School”, National Graduate School of Scientific Computing, Stockholm, August 18, 2003 (and August 19, 2002).
- Michael Hammill, “Introduction to Programming with Python”, National Graduate School of Scientific Computing, Stockholm, August 18, 2003 (and August 20, 2000, August 19, 2002).
- S. Lennart Johnsson: “Introduction to Grid Computing”, National Graduate School of Scientific Computing, Stockholm, August 18, 2003.
- S. Lennart Johnsson: “High-Performance Software for Scientific Simulations in Grid Environments: Adaptive Software Systems”, Australian National University and Australian Partnership for Advanced Computing, Canberra, Australia, July 10, 2003.
- S. Lennart Johnsson: “Grid deployment and support – the NGC, EGSC and SweGrid initiatives”, Australian National University and Australian Partnership for Advanced Computing, Canberra, Australia, July 10, 2003.
- S. Lennart Johnsson: “High Performance Software for Scientific Simulations in Grid environments: Adaptive Software Systems”, ICIAM 2003, Sydney, Australia, July 7 - 11, 2003.

- S. Lennart Johnsson: “TIGRE – Applications and Technology candidate projects”, HiPCAT, Austin, TX, June 30, 2003.
- Lars Forsberg. “NeuroViz – A visualizer for the NeuroGenerator database”, 9th Annual Meeting of the Organization for Human Brain Mapping, New York, June 18-22, 2003.
- Gert Svensson, Lars Forsberg, Anders Selander with Per Roland, Tony Lindeberg, Tore Risch, Christian Engström, Jesper Fredriksson, Mikael Naeslund, Johan Sandström, and Calle Undeman, “The NeuroGenerator database – current status”, The 9th Annual Meeting of the Organization for Human Brain Mapping, New York, June 18-22, 2003.
- S. Lennart Johnsson: “Grid deployment and support – the NGC, EGSC and SweGrid initiatives”, The EU eInfrastructures Initiative: Towards integrated Networking and Grids infrastructures for eScience and beyond, Athens, June 12, 2003.
- Gert Svensson, Lars Forsberg, ”NeuroGenerator – en databas för att kunna se tankar”, Riksutställningar – Swedish Travelling Exhibitions, June 3, 2003.
- S. Lennart Johnsson: “Grids, Applications and Performance”, Performance Workshop, Stockholm, May 27, 2003.
- S. Lennart Johnsson: “Grids - Drivers (Applications) and Challenges”, HP Enterprise Users Week, Amsterdam, May 20, 2003.
- Gert Svensson, “The VR-Cube”, Swedish Audio Engineering Society, May 20, 2003.
- S. Lennart Johnsson: “Bio-Imaging”, Rice University, Houston, May 7 - 8, 2003.
- Olle Mulmo: “European Grid Support Centre”. The 6th European DataGrid conference, Barcelona, May 2003.
- S. Lennart Johnsson: “Grid Research at PDC”, Swedish Institute for Computer Science, Stockholm, April 11, 2003.
- S. Lennart Johnsson: “Unleashing the Power of Processing”, KTH, Stockholm, April 10, 2003.
- S. Lennart Johnsson: “STAC: SNIC’s Strategic Technology Advisory Committee”, SweGrid, Uppsala, April 9, 2003.
- Olle Mulmo: “Globus: middleware för superdatorer”. The 8th Trefpunkt conference, Linköping, April 2003.
- S. Lennart Johnsson: “Research in High-Performance Grid Software”, The Swedish Research Council’s Grid Research Kick-off Meeting, March 11, 2003.
- S. Lennart Johnsson: “Simulation Science in Grid Environments: Integrated Adaptive Software Systems”, Hayama, Japan, March 4 - 7, 2003.

- S. Lennart Johnsson: “Adaptive Scientific Software Libraries”, Los Alamos Computer Science Institute, Los Alamos, NM, February 26, 2003.
- S. Lennart Johnsson: “TLC2 Infrastructure Efforts and Grid Research”, Texas Learning and Computation Center Bioimaging Initiative, Houston, TX, February 18, 2003.
- S. Lennart Johnsson: “The European Grid Support Center: Mission and Plans”, Abingdon, UK, February 10 - 11, 2003.
- Olle Mulmo: “Globus in a Kerberized environment”. Presentation at the GlobusWORLD conference, San Diego, January 2003.
- Olle Mulmo: “Authorization in the European DataGrid”. Presentation at the GlobusWORLD conference, San Diego, January 2003.
- Olle Mulmo: “Grids and WS-Security”. Panelist at the GlobusWORLD conference, San Diego, January 2003.
- Ulf Andersson, “Benchmarking on the Itanium 2 Cluster at PDC”, LCSC 2003, 4th Annual Workshop on Linux Clusters for Super Computing, Linköping, 2003.
- Kai-Mikael Jää-Aro, “Implementing a CFD steering system for immersive environments”, at CAVE Programming Workshop 2003.
- Gert Svensson and Kai-Mikael Jää-Aro, “VIRTUALFIRES – realtidssimulering och visualisering av brandförlopp i tunnlar”, VR-FORUM 2003.
- Gert Svensson, “The VR-Cube”, Association of Interacting Arts, December 3, 2002
- S. Lennart Johnsson: “Adaptive Scientific Software Libraries”, SANS Summit, Knoxville, TN, August 7 - 8, 2002.
- Gert Svensson, “Virtual Reality at PDC”, Electronic Visualization Laboratory, University of Illinois at Chicago, August 7, 2002.
- Olle Mulmo: “Grid Computing”. Presentation at the PDC summer school, August 2002.
- S. Lennart Johnsson: “The Texas Learning and Computation Center”, College of Engineering, University of Houston, July 12, 2002.
- S. Lennart Johnsson: “Computational and Information Grids - An Approach to Code Portability”, Institute of Computer Science, Foundation of Research, Hellas, Crete, July 4, 2002.
- Gert Svensson, Lars Forsberg, “The Neurogenerator Submission Procedure and User Interface”, The 8th Annual Meeting of the Organization for Human Brain Mapping, Sendai, June 2-6, 2002.
- S. Lennart Johnsson: “Grids: Next Generation Infrastructure for Research, Education and Commerce”, Swedish Ministry of Education, Stockholm, May 27, 2002.

- S. Lennart Johnsson: “The Nordic Grid Consortium”, NorduGrid, Helsinki, May 23 - 24, 2002.
- Olle Mulmo: “The Globus Project - a perspective”. The 3rd NorduGrid Woshop, Helsinki, May 2002.
- S. Lennart Johnsson: “Texas learning and Computation Center: Grid Research”, University of Houston Board Meeting, April 30, 2002.
- S. Lennart Johnsson: “Grid: Projects, Ambitions and Challenges”, Notur, Bergen, April 25 - 26, 2002.
- S. Lennart Johnsson: “The Nordic Grid Consortium”, the 2002 NorduNet Conference, Copenhagen, April 15 - 17, 2002.
- S. Lennart Johnsson: “Simulation and Analysis without bounds - Enabling Technologies”, Shell Conference, The Woodlands, TX, April 10, 2002.
- Per Öster: “ENSCUBE - a collaborative effort for supercomputing throughout the supply chain”, International Partnerships Engineering Group, SAAB Systems and Electronics, Stockholm, March 21, 2002.
- S. Lennart Johnsson: “Application and Platform Adaptive Scientific Software”, NCSA, Urbana/Champaign, March 14, 2002.
- S. Lennart Johnsson: “Data and Computation Grids”, The Texas Telecommunications Infrastructure Fund, Houston, TX, March 1, 2002.
- Per Öster: “Shift in the HPC user community”, NPACI All Hands Meeting, San Diego, March 2002.
- S. Lennart Johnsson: “Grid Computing”, The Swedish Research Council, Stockholm, February 8, 2002.
- S. Lennart Johnsson: “Grid Projects”, The Swedish Research Council, Stockholm, February 8, 2002.
- Gert Svensson, “Virtual Reality”, Baltic Art Workshop, February 8, 2002.
- S. Lennart Johnsson: “Grid Projects”, Center for Scientific Computing, Helsinki, February 4, 2002.
- S. Lennart Johnsson: “Computing: The Next Decade”, Keck Center for Computational Biology, Houston, TX, February 1, 2002.
- S. Lennart Johnsson: “Computing: The Next Decade”, Texas Learning and Computation Center, Bioimage Research Group, January 24, 2002.
- S. Lennart Johnsson: “PDC, Grids and Open Source Software”, The European Commission, Brussels, December 17, 2001.
- Gert Svensson, “High-Performance Computing in Sweden”, Norwegian Supercomputing Board, December 4, 2001.
- S. Lennart Johnsson: “Computational Grids and HPC - The Ultimate Environment for code portability and adaptivity”, Rensselaer Polytechnic Institute, Albany, NY, November 20, 2001.

- S. Lennart Johnsson: "Computational Grids and HPC - The Ultimate Environment for code portability and adaptivity", NEC Research Institute, Princeton, NJ, November 19, 2001.
- S. Lennart Johnsson: "Computing: The Next Decade", Baylor College of Medicine, Structural Computational Biology and Molecular Biophysics, November 16, 2001.
- Gert Svensson, "Activities at PDC", Swedish Space Cooperation - Esrange, October 23, 2001.
- S. Lennart Johnsson: "Adaptive High Performance Numerical Components: A design and implementation methodology", Los Alamos Computer Science Institute, Santa Fe, NM, October 15, 2001.
- Gert Svensson, "Virtual Reality", Djurgårdsförvaltningen, August 30, 2001.
- S. Lennart Johnsson: "Computational Science in the 21st Century", Royal Institute of Technology, Stockholm, Sweden, August 20 - 31, 2001.
- S. Lennart Johnsson: "Parallel Algorithms", PDC Summer School in High Performance Computation, Royal Institute of Technology, Stockholm, August 20 - 31, 2001.
- S. Lennart Johnsson: "GrADS: Grid Application Development Software", University of Texas, Austin, July 24, 2001.
- S. Lennart Johnsson: "GrADS: Grid Application Development Software", 15th ACM International Conference on Supercomputing, Sorrento, Italy, June 16 - 21, 2001.
- S. Lennart Johnsson: "Grid Application Development - The Ultimate Challenge for Code Portability and Adaptivity", Dagstuhl Seminar "Management of Metacomputers", Dagstuhl, Germany, June 10 - 15, 2001.
- Gert Svensson with Peter Lunden and Johan Vävare, "Design of the Sound System at the PDC VR-CUBE at the Royal Institute of Technology", Acoustic Rendering for Virtual Environments, SnowBird, Utah, USA, May 26th-29th, 2001.
- S. Lennart Johnsson: "Computational Grids and High-Performance Computation: The ultimate environment for code portability and adaptivity", University of Southern California, Los Angeles, March 30, 2001.
- Gert Svensson, "Activities at PDC", European Joint Research Council, March 16, 2001.
- S. Lennart Johnsson: "Computational Grids and High-Performance Computation: The ultimate environment for code portability and adaptivity", the Mardi Gras 2001 Conference, Baton Rouge, LA, February 22 - 24, 2001.
- S. Lennart Johnsson: "Computational and Information Grids - A US Perspective", The Swedish Research Council, Stockholm, Sweden, February 15, 2001.

- S. Lennart Johnsson: “The KTH Linux Laboratory: An Open Source Development Laboratory”, Royal Institute of Technology, Stockholm, February 13, 2001.
- S. Lennart Johnsson: “Computational Grids and High-Performance Computation: The ultimate environment for code portability and adaptivity”, University of Chicago, Chicago, February 5, 2001.
- Per Öster: “HPC In Northern Europe”, NPACI All Hands Meeting, San Diego, February 2001.
- S. Lennart Johnsson: “Computational Grids and High-Performance Computation: The ultimate environment for code portability and adaptivity”, University of Illinois at Chicago, Chicago, January 29, 2001.
- S. Lennart Johnsson: “Education in Computational Science and Engineering: What Must be Done?”, Arcade 2000, Bergen, Norway, November 27 - 28, 2000.
- Michael Hammill, “MPI Derived Data Types and Virtual Topologies”, PDC Summer School in High Performance Computation, Royal Institute of Technology, Stockholm, August 28, 2000.
- S. Lennart Johnsson: “Parallel Algorithms”, PDC Summer School in High Performance Computation, Royal Institute of Technology, Stockholm, August 21 – September 1, 2000.
- Michael Hammill, “Programming Languages: C++”, PDC Summer School in High Performance Computation, Royal Institute of Technology, Stockholm, August 20, 2000.
- S. Lennart Johnsson: “GEMSViz”, iGrid2002, Yokohama, July 18 - 21, 2000.
- Gert Svensson: “Visualisation in the Future”, Ericsson System Projects, May 4, 2000.
- Gert Svensson: ”Visualisering för arkitekter”, Helsingborg, LTH, May 2, 2000.
- Gert Svensson: ”Visualisering för arkitekter”, Virtuellt verklighet i kubik – Workshop for architects, Building Research Council, April 13, 2000.
- S. Lennart Johnsson: “SimDB: A Problem Solving Environment for Molecular Dynamics Simulation and Analysis”, First European Grid Forum, Poznan, Poland, April 11 - 13, 2000.
- Gert Svensson: “The 3Demo project – Visualization for Architects”, Visualising the Future workshop, London, March 23, 2000.